Potassium interactions with copper slag and magnetite fines in chemical-looping processes

Fuel Processing Technology 270 (2025) 108192

Contents lists available at ScienceDirect

Fuel Processing Technology

journal homepage: www.elsevier.com/locate/fuproc

Potassium interactions with copper slag and magnetite fines in chemical-looping processes

Felicia Störner [a,*], Ivana Staničić [a], Pavleta Knutsson [b], Tobias Mattisson [a], Magnus Rydén [a]

[a] Chalmers University of Technology, Department of Space, Earth and Environment, Hörsalsvägen 7B, SE-412 96 Göteborg, Sweden
[b] Chalmers University of Technology, Chemistry and Chemical Engineering, Kemigården 4, SE-412 96 Göteborg, Sweden

ARTICLE INFO

Keywords:
Chemical-looping combustion
Oxygen carrier aided combustion
Ash interactions
Potassium interactions
iron oxide
Oxygen carrier

ABSTRACT

Using oxygen-carrying bed materials is a promising alternative to conventional fluidized bed combustion. Biomass-derived fuels contain ash rich in K and P, which might react with the oxygen carrier, leading to agglomeration and other problems. This study investigates the performance of copper slag (Järnsand, Fe-Si-oxide) and magnetite fines (MAF, Fe_3O_4) as oxygen carriers in a lab-scale fluidized bed reactor with subsequent material analysis. The conversion of methane and the fluidization was monitored, as K_2CO_3 or KH_2PO_4 was added as ash model compound. The fuel conversion was mainly unaffected by K-salt addition, apart from when K_2CO_3 was added to MAF at 950 °C and the conversion increased, along with increased porosity. Järnsand captured K from K_2CO_3. Mg and Al inherent to Järnsand participated in the interaction, contributing to increasing the melting point of the formed K-silicates. In MAF, the uptake of K was low: thermodynamic calculations suggested the formation of $KFe_{11}O_{17}$ and small amounts of slag. KH_2PO_4 always caused agglomeration by a melt-induced mechanism. The K-P-melt absorbed Fe in MAF or Ca in Järnsand. In conclusion, Järnsand seems like a promising oxygen carrier for biomass-derived fuels, while MAF might suffer from poor particle integrity in the presence of K-rich ash species.

1. Background

Oxygen carriers are materials containing transition metal oxides that, at their oxidized state, can oxidize fuel at typical fluidized-bed combustion conditions. Subsequently, at their reduced state, they can be re-oxidized using air. This cyclic reduction and oxidation mechanism can be applied to both combustion and gasification processes [1].

Traditionally, oxygen carrier development has focused on Chemical-Looping Combustion (CLC). In CLC, the oxygen carrier is oxidized with air in an air reactor and the fuel is converted by reducing the oxygen carrier in a separate fuel reactor. The concept is illustrated in Fig. 1. This results in a process where the air is not in direct contact with the combustion products (CO_2 and steam), meaning that CO_2 capture is possible to realize without major gas separation processes. Autothermal CLC has been demonstrated at a 5 MW scale with coal and pet coke [2,3] and solid fuel biomass-CLC has been demonstrated in a 1 MW pilot plant in TU Darmstadt [4]. Truly industrial-size CLC is yet to be demonstrated, but a few boiler designs have been suggested. For example, the design and cost estimation of 200 MW_{th} [5] and 1000 MW_{th} [6] solid-fuel CLC boilers have been proposed by Lyngfelt and colleagues. Several hundred different oxygen carriers, both naturally occurring and synthetic, have been suggested and evaluated for CLC applications [7]. The oxygen carriers considered in this study are based on iron oxide, which has many advantages and is a common choice. The oxygen carrying properties of iron oxide in CLC and OCAC is attributed to the transition between Fe_2O_3 (hematite) and Fe_3O_4 (magnetite). A deeper reduction (i.e. the formation of FeO and elemental Fe) is not desirable and might result in sintering [8].

A related application of oxygen carriers is Oxygen Carrier Aided Combustion (OCAC). OCAC involves the use of oxygen carriers as bed material in conventional fluidized bed combustion (FBC). FBC is a well-established technology for the thermal conversion of coal, solid biomass, and waste-derived fuels [9], and the difference between conventional FBC and OCAC is illustrated in Fig. 2. In OCAC, the oxidation and

Abbreviations: CLC, Chemical Looping Combustion; OCAC, Oxygen Carrier Aided Combustion; FBC, Fluidized Bed Combustion; MAF, Magnetite Fines; SEM, Scanning Electron Microscopy; EDS, Energy Dispersive X-Ray Spectroscopy; XRF, X-Ray Fluorescence Spectroscopy; FAAS, Flame Atomic Absorption Spectroscopy; ICP-MS, Inductively Coupled Plasma Mass Spectrometry.

* Corresponding author.
E-mail address: felicia.storner@chalmers.se (F. Störner).

https://doi.org/10.1016/j.fuproc.2025.108192
Received 3 September 2024; Received in revised form 6 February 2025; Accepted 13 February 2025
Available online 20 February 2025

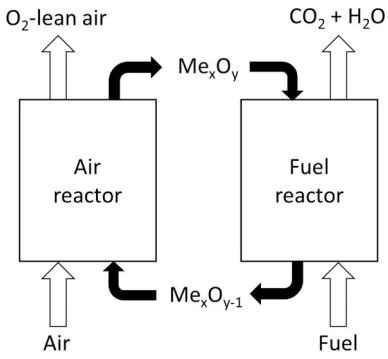

Fig. 1. Illustration of the Chemical-Looping Combustion (CLC) process.

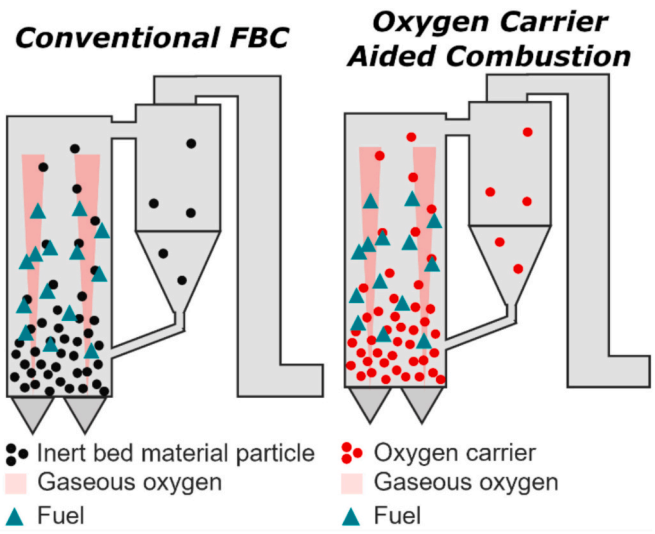

Fig. 2. Schematic representation highlighting the main differences between conventional FBC (left) and OCAC (right).

reduction are not separated into two reactors but happen at different locations in the furnace, where the atmosphere can be either reducing or oxidizing depending on the location. Especially when using a high-volatile fuel such as biomass, the fast release of volatiles creates a pronounced reducing zone close to the fuel-feeding location [10]. It can thus be expected that bed particles are exposed to alternating reducing and oxidizing conditions and that the oxygen carrier is subject to similar reactions and changes in oxidation state as in CLC.

Utilizing an oxygen carrier in FBC creates an oxygen buffer in the bed [10–12], which enables operation at a lower air surplus than conventional FBC, in turn resulting in higher thermal efficiency and allowing for increased thermal load. The accumulated experience with industrial-scale OCAC has been summarized by Störner et al. [13], and boilers up to 350 MW_{th} have been operated commercially with ilmenite as bed material [14,15]. Higher operation temperatures, lower fluidization gas velocities, and lower air surplus have been achieved by replacing the silica sand bed with rock ilmenite, resulting in up to a 7 % increase in thermal capacity [14]. However, the high cost of ilmenite and the desire to limit the utilization of primary resources in general has led to an increased interest in instead using by-products from metallurgical industries as oxygen carrying bed material [13,16,17].

The presence of reactive ash species in biomass is a common problem in FBC. Interactions between ash species and oxygen carriers is a relevant aspect also for CLC and OCAC applications but is not yet well understood. It can be expected that K, Na, and P-species could interact with oxygen carrier materials and that a high regeneration rate of bed material will likely be required. The current study aims to provide an understanding of how certain oxygen carriers perform in the presence of K- and P-rich components.

This study explores the utilization of two iron-oxide based oxygen carriers: copper smelter slag and magnetite fines (MAF). Copper smelter slag in an iron-rich by-product of the copper smelting process. It's produced at large quantities that are currently not fully utilized [13]. The oxygen-carrying properties of the copper smelter product Järnsand ("iron sand") have been investigated briefly, and fluidization properties and reactivity with fuel have been confirmed [18]. The amount of research is however still scarce and ash interactions with relevant ash concentrations have not been studied. MAF is a primary ore product with a very high magnetite content. MAF is a key intermediate product in the European iron and steel industry and is available in excessive amounts [13]. The high iron oxide content makes it promising as an oxygen carrier and makes it a suitable model material to study for an increased understanding of the interactions between iron oxide and biomass ash. An advantage for both MAF and Järnsand is that the products are already in the form of particles with size distributions overlapping with common FBC-bed materials.

1.1. Ash interactions with oxygen carriers

The ash composition of the fuel has a great impact on the thermal conversion process. Depending on fuel and combustion conditions, the ash can cause problems like emissions, slagging, fouling on heat-transfer surfaces, agglomeration of bed material, and inhibition of complete fuel burnout [19–23]. In biomass conversion, alkali plays an important role in the ash chemistry. Ideally, the alkali from the fuel is absorbed efficiently by the bed material without causing problems related to fluidization or emissions. If, however, the bed material quickly gets saturated with alkali, or if the alkali causes the material to agglomerate rapidly, a high replacement rate of bed material is required. The most used bed material in FBC is silica sand. Alkali interactions with silica sand cause bed agglomeration [23,24], which means it has to be continuously replaced. Silica sand has a low cost, so a high bed regeneration rate can be applied. This might not be the case for oxygen carriers, which can be assumed to be more expensive [13].

Agglomeration is typically caused by the presence of a sticky phase on the particle surface, causing particles to adhere together. Two main mechanisms have been suggested: coating-induced and melt-induced agglomeration [25,26]. Coating-induced agglomeration is initiated when the interaction between ash species and bed material results in the formation of sticky phases. This mechanism thus depends on both ash and bed material compositions and ash layers can grow inwards into the particle [25]. Melt-induced agglomeration is when a sticky phase is formed solely through interactions between ash species. This phase subsequently adheres to the bed particle surface when they collide. This causes ash layers to build mainly outwards from the surface. The two mechanisms were exemplified by Sevonius et al. [27] by studying the interactions between SiO_2 (bed material) and different K-salts (ash model compounds) in fluidized bed experiments at oxidizing conditions. They saw that KCl caused agglomeration by KCl-melt adhering directly onto the particle surface (melt-induced agglomeration). K_2CO_3, on the other hand, reacted with the SiO_2-based bed material to form a sticky K-silicate (coating-induced agglomeration).

The bed particle can be considered inert in melt-induced agglomeration but reactive in coating-induced agglomeration. However, interactions might also take place without inducing agglomeration. Lab-scale fluidized bed experiments (under oxidizing conditions [28] and under alternating reducing and oxidizing conditions [29,30]) and industrial-scale experiments with ilmenite have shown that K is readily captured in the core of the particles with the formation of stable K-titanates. Ilmenite is thus resistant to coating-induced agglomeration. The addition of KH_2PO_4 in experiments, however, readily caused melt-induced agglomeration. A melt-induced layer formation can thus be a cause for agglomeration even though the interaction with the material

itself is either limited or results in non-sticky phases, such as K-titanates. The agglomeration resistance has a large impact on the bed material consumption. Lind et al. [31] studied different bed materials in a 75 MW and an 85 MW municipal solid waste-fired CFB. With silica sand, the bed regeneration rate was typically 6 kg/MWh. With ilmenite as bed material, on the other hand, the make-up rate could be reduced to 3, or even down to 1 kg/MWh, while still observing the positive oxygen-carrying effect.

Since Si readily reacts with K, Si-based materials are at risk of agglomerating with biomass fuels in a similar way as has been observed in conventional FBC using sand. However, depending on the composition of the bed material, even Si-containing materials can have some resistance to agglomeration. Faust et al. [32] studied different Si-phases and their interactions with woody biomass ash in dual fluidized bed gasification. They saw that materials with highly polymerized Si-structures, such as quartz and feldspar, interacted readily with K to form $K_2Si_4O_9$, which has a melting point of 771 °C. The materials with less polymerized Si-structure (like $CaSiO_3$ and $MgFeSiO_4$) showed less interaction with K. Ca was instead more likely to be incorporated in those materials and no melt was formed. Similar results were reported by Bozaghian et al. [33], who studied barley straw ash interactions with quartz, K-feldspar and olivine. In general, elements responsible for forming phases with low melting points are mainly K, P, Na, and S-species, while ash (or ash interaction products) rich in Ca, Mg, and Al have higher melting temperatures [26,34].

Studies on the ash interactions with copper smelter slag are very limited as of today and to the best of our knowledge, no studies of ash interactions with MAF have been presented in the scientific literature. Alkali interactions with more or less pure Fe-oxides in fixed bed experiments include a study on iron mill scale (Glödskal) [35] and a study on pure Fe_2O_3 and pure Fe_3O_4 [36]. In both cases, the absorption of K was generally very low, but the formation of K_2FeO_4 was observed in the interaction between KNO_3 and Fe_2O_3 [36]. In both studies, the presence of KH_2PO_4 caused agglomeration, due to the melting of its decomposition product, KPO_3. Thermodynamic modelling of interactions between Fe_2O_3 and three biomass-derived fuels was done by Staničić et al. [37] and they predicted the formation of K_2O- and KPO_3-slag phases and alkali silicates, where Si originated from the fuel itself. No K-Fe-oxide phases were predicted.

1.1.1. Potassium salts as ash model compounds in ash interaction studies

The ash interaction chemistry in biomass-derived fuel combustion is very complex, where several reactions compete and happen on different time scales. Knowledge about the elemental composition alone is not sufficient to predict the outcome and in many studies, ash interactions have therefore instead been mimicked by the use of ash model compounds in the form of pure salts or mixtures of a few salts [28,36,38–41]. When using model compounds, the reaction system becomes very much simplified, parameters are more easily controlled, and reaction mechanisms can be studied in more detail.

The reason for focusing on K-compounds is that they are responsible for many of the undesirable ash interactions in boilers [19,23]. In biomass, K is typically present in the form of soluble salts, or organically bound to the char matrix. The release and subsequent transformations of K have been explored in many previous studies by studying bed material samples [20,42,43], and by monitoring gas phase alkali [44–46]. K speciation is complex and depending on what counter ions are available, K may be present in the form of mainly KCl(g), KOH(g), K_2SO_4 (in oxidizing conditions), and K(g) (in reducing conditions) in combustion settings. These species may then be transformed both in the gas phase as well as in reaction with solids or liquids in secondary processes.

Choosing suitable ash model compounds is crucial for obtaining representative results in experimental studies. In the current study, K_2CO_3 and KH_2PO_4 were used as ash model compounds. Although K_2CO_3 is not likely a significant form of K in combustion conditions, using it as a model compound for K-interactions is useful for a couple of reasons. K_2CO_3 is expected to decomposes to some extent to K_2O, which is volatile and more reactive. However, it's expected to be stable enough to reach the fluidized bed in solid form in the experiment and have a significant residence time inside the bed, based on previous experiments [29]. The release of K from K_2CO_3 and different biomasses and salt mixtures with varying Cl- and S-content was investigated by Knudsen et al. [47]. K was present as K_2CO_3 in the temperature interval 500–950 °C in Si-lean ash. The carbonate fraction decreased at temperatures above 700–800 °C because of the decomposition of K_2CO_3 in the presence of small amounts of H_2O and CO_2. High partial pressures of CO_2 shift the equilibrium towards K_2CO_3 being more stable, however, the effect of CO_2 presence is low above 900 °C. [48]. For the present experimental setup, the behaviour of K_2CO_3 is discussed in more detail in Section 3.1 below. Further, K_2CO_3 has a melting point of 891 °C, and by conducting the experiments at both 850 and 950 °C, it is simulated how the direct melting of the ash species might affect the bed of oxygen carriers.

Other K-species such as KCl and KOH are highly volatile under the experimental conditions and using them instead would likely result in very short interaction times [28,35]. K_2SO_4, on the other hand, is also expected to have very little interaction due to its high stability under combustion conditions [28,35]. For instance, the addition of S during biomass combustion is an effective way of forming K_2SO_4 to avoid K interactions in the combustion chamber in FBC [49].

P-rich fuels such as sewage sludge and various agricultural residues might become important energy sources when the competition over woody biomass increases [43,50]. If P is present together with alkali, alkali-phosphates can form [42,43], which is modelled in this study by KH_2PO_4. It's been found that with P, the alkali distribution changes and KCl and K-silicates are replaced by Ca/Mg-K-P species with higher melting temperatures in the course fly ash [43]. In this way, P could have a positive effect on e.g. slagging and agglomeration. However, if P the concentration become excessive with regards to Ca and Mg, it might instead form KPO_3 and $K_5P_3O_{10}$ with low melting temperatures, leading to agglomeration. It is thus evident that K—P interactions may affect the boiler operation and are important to understand in the utilization of Fe-oxide oxygen carriers. Still, the Fe-K-P system is not well studied. KH_2PO_4 has a melting temperature of 253 °C and decomposes upon heating into KPO_3 and H_2O. KPO_3 has a melting temperature of 807 °C and sticks to particle surfaces, which is why experiments with KH_2PO_4 have resulted in agglomeration in several different oxygen carriers [28,35,36,38]. Lidman Olsson et al. [51] studied the interaction between ilmenite and Na-phytate and found that the agglomeration tendency probably depended on the initial porosity of the ilmenite particles. They also found that the interactions negatively affected the fuel reactivity of ilmenite. The fact that limited experiments have been conducted with P-compounds on oxygen carriers, an no studies with copper smelter slag and MAF, motivates further studies.

1.2. Aim of the study

This experimental study aimed to investigate the performance of two oxygen carriers, copper smelter slag (Järnsand) and magnetite fines (MAF), at conditions relevant to OCAC and CLC. The accumulation of K- and P-rich fuel ash during combustion was simulated by adding ash model compounds (K_2CO_3 and KH_2PO_4) while simultaneously subjecting the materials to reduction-oxidation cycles. The methodology was developed and used with ilmenite as an oxygen carrier in a previous study [29] where the fuel conversion and agglomeration of ilmenite in the presence of K_2CO_3 during fluidization was studied.

The materials were evaluated concerning fluidization, reactivity with methane and oxygen, and interactions with K and P from the ash compounds. Morphological and compositional changes were studied by material analysis (SEM-EDS). The goal was to determine whether the oxygen carriers would be suitable for converting biomass-derived fuels, or if the ash interactions would result in deactivation or severe

agglomeration. Although ash interactions with similar materials have already been studied, much of the published literature presents experiments in either a fixed bed or in a fluidized bed with only oxidizing conditions or very low ash concentrations. The novelty of this work is that it combines the aspects of fluidization, varying atmosphere (reducing and oxidizing) and addition of ash compounds in the same experiment, which will mimic most closely the real industrial-scale conditions.

2. Method

2.1. Experimental setup

The experiments were conducted in a fluidized bed reactor located inside an electrically heated furnace. A schematic description of the reactor is shown in Fig. 3. This unit was presented in an earlier study, with the main goal of being able to effectively study the fuel conversion of oxygen carriers in the presence of solid ash species under relevant, fluidized conditions [29].

The reactor is constructed from two vertical 253MA steel pipes with an inner diameter of 26 mm. A distribution plate made of perforated stainless steel is located between the pipes. The plate supports the bed material and distributes the gas which is supplied at the bottom of the reactor. The amount of bed material in the experiments was 20 g, which resulted in an unfluidized bed height of 2.24 cm for Järnsand and 1.46 cm for MAF. The gas is supplied in a gas line via magnetic valves, to allow for quick switching between different gas mixtures. The top pipe, housing the bed and the freeboard is 270 mm long. The top of the reactor is equipped with a gas line for the outlet and an airlock for feeding solid particles to the bed. The airlock has a connection for the sweep gas. The exiting gas is cooled and enters a gas analyser measuring the concentrations of CH_4, CO, CO_2, and O_2. The pressure drop over the reactor is continuously measured at a frequency of 10 Hz. Two thermocouples monitor the temperature below and inside the bed. The reactor and the surrounding experimental infrastructure are explained in more detail by Störner et al. [29] and by Leion et al. [52], respectively.

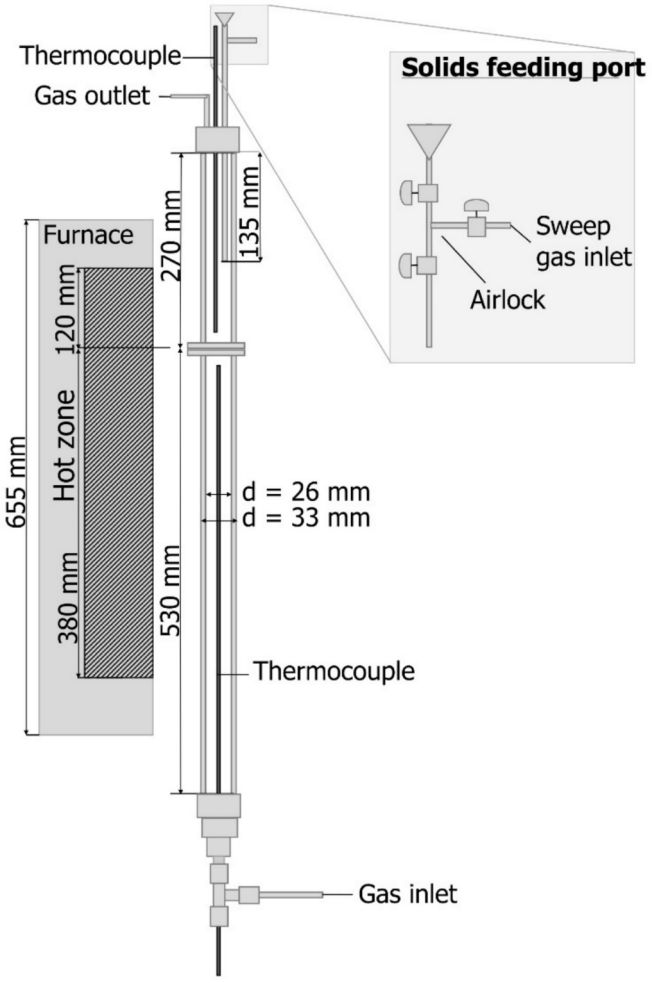

Fig. 3. Schematic representation of the steel reactor and the electric furnace used in the current experimental setup.

2.2. Fuel conversion experiments with salt addition

Each experiment consisted of several reduction-oxidation cycles. One such cycle consisted of periods of inert, reducing, inert, and oxidizing gas environments, where the reduction represents the fuel reactor in CLC or the local reducing conditions in OCAC. Conversely, the oxidation represents the air reactor or the oxygen-rich areas in the boiler. In this way, the material was exposed to conditions which would be expected both in CLC and OCAC, albeit the time scales and degrees of reduction may be different. Details are provided in Table 1. Inert periods are used between oxidation and reduction to purge the reactor.

The oxygen carrier was added, and the reactor was heated in oxidizing conditions. Once the experimental temperature was reached, the environment was switched to inert, initiating the first reduction-oxidation cycle. A 400/500 NmL/min mixture of CH_4/N_2 was then used for reducing conditions. A low CH_4 conversion is expected with iron-based oxygen carriers [29,53], and using CH_4 is therefore suitable for studying how the reactivity differs at different conditions. After the reduction followed a period of inert gas, and then the material was oxidized. The last cycle ended at the reducing period, and the reactor was then cooled down in inert atmosphere. Thus, the particles subsequently extracted from the reactor for analysis were at their reduced state. Salt addition was initiated at the beginning of the sixth cycle, during the inert period. The amounts of salt added, and the corresponding cycle number are presented in Table 2. The amounts are based on previous studies [28,29], and the method was designed to simulate both a low, initial ash exposure and the expected maximum exposure in boiler settings during a reasonable experiment time. During the whole experiment, 500 NmL/min N_2 was added as a sweep gas to transport the salt particles into the reactor. In a previous study, it was concluded that the sweep gas did not interfere with the fuel conversion [29]. The minimum fluidization velocity of Järnsand and MAF is estimated to be 0.009 and 0.014 m/s, respectively, during the experiments (after material preparation according to Section 2.3.3 below). The superficial gas velocity in the experiments was between 0.11 and 0.13 m/s.

The salt was added every second cycle, allowing the in-between

Table 1
Gas compositions and time durations for the experiment cycles with diluted methane as fuel.

Period	Gas flow (NmL/min)	Gas composition	Time
Heating	1000 NmL/min	Air in N_2 (12.4 % O_2)	
Start of experimental cycles			
Inert*	1000 NmL/min	N_2	180 s (approx.)
Reduction	400 NmL/min	CH_4	40 s
	500 NmL/min	N_2	
Inert	1000 NmL /min	N_2	60 s (approx.)
Oxidation	1000 NmL/min	Air in N_2 (12.4 % O_2)	Until outlet = inlet O_2 concentration

* K_2CO_3 or KH_2PO_4 was added to the bed during this inert period preceding the reduction An additional 500 NmL/min N_2 was added at the top of the reactor as sweeping gas during the whole experiment.

Table 2
K_2CO_3 and KH_2PO_4 addition amounts and corresponding cycle number.

Cycle no.	Addition (mg)	Acc. (mg)	Addition (mg)	Acc. (mg)
	K_2CO_3		KH_2PO_4	
	T_melt = 891 °C		T_melt = 810 °C (KPO_3)	
	Particle size = 250–850 μm		Particle size = 250–850 μm	
6	60	60	15	15
8	60	120	15	30
10	120	240	15	45
12	120	460	20	65
14	150	610	30	95
16	300	910	60	155
18	300	1210	80	235

cycles to be used for evaluation of fuel conversion without disturbance by salt addition e.g. release of CO_2 from K_2CO_3. The addition of KH_2PO_4 to the bed was done at a much lower rate than K_2CO_3 based on previous experiences with KH_2PO_4 causing severe agglomeration in ilmenite and silica sand beds already at low concentration [27,28]. The total addition of 1210 mg K_2CO_3 adds 690 mg of K to the bed, which amounts to 3.45 wt.-% of the total bed weight (based on the initial, calcined material). The introduction of 235 mg KH_2PO_4 adds 67 mg K, or 0.335 % of the total bed weight. The K_2CO_3 and KH_2PO_4 were provided by Sigma Aldrich and had a > 99 % purity. The salts were added as-is, without any sieving or grinding as preparation.

Each experiment was conducted with the addition of either K_2CO_3 or KH_2PO_4 at 950 or 850 °C, resulting in 12 experiments including reference experiments with no salt addition. The experiments and their corresponding samples will be referred to in the text according to the abbreviations given in Table 3.

2.3. Materials

2.3.1. Järnsand - copper slag from Boliden

The copper slag studied in this work is a water-granulated slag originating from Boliden AB. Boliden produces in total around 1.5 million tons of slag annually in Sweden and Finland, and a significant amount of that (around 250–270 kton in Sweden) is water granulated, which produces glassy particles of sizes up to 4 mm. Water granulation is done by quickly quenching the slag with water, thus, water granulated slag is largely amorphous. The slag is commercialized with the Swedish product name Järnsand. The oxygen carrier used in this work is derived from a product with particles up to 2 mm in size which is used as construction aggregate, abrasive media, and various other applications [13].

The elemental composition of the provided material had been analyzed with a combination of X-Ray Fluorescence (XRF) and Flame Atomic Absorption Spectroscopy (FAAS) and is presented in Table 4. The composition gives a molar Fe:Si ratio of about 1:1. A bulk density of 1.675 g/cm^3 was measured using a standard Funnel method (ISO 3923-1:2008).

Table 3
The designations given to the experiments and their corresponding samples.

Salt addition	Temperature [°C]	Oxygen carrier	Designation
None	850	Järnsand	JS_ref_850
None	950	Järnsand	JS_ref_950
K_2CO_3	850	Järnsand	JS_K_2CO_3_850
K_2CO_3	950	Järnsand	JS_ K_2CO_3_950
KH_2PO_4	850	Järnsand	JS_KH_2PO_4_850
KH_2PO_4	950	Järnsand	JS_ KH_2PO_4_950
None	850	MAF	MAF_ref_850
None	950	MAF	MAF_ref_950
K_2CO_3	850	MAF	MAF_ K_2CO_3_850
K_2CO_3	950	MAF	MAF_ K_2CO_3_950
KH_2PO_4	850	MAF	MAF_ KH_2PO_4_850
KH_2PO_4	950	MAF	MAF_ KH_2PO_4_950

The granulated material could, based on its composition and size distribution, be suitable to use as a bed material for fluidized bed conversion processes. Since Järnsand is a by-product with limited overall utilization as of today, utilizing it instead of a virgin material such as an ore or silica sand makes sense from a resource utilization perspective [13].

2.3.2. MAF - Magnetite fines from LKAB

The second oxygen carrier studied in this work is magnetite fines (MAF), which is an enriched iron ore product produced by LKAB. MAF is used for sintering into pellets that, in turn, are smelted into iron in the blast furnace.

MAF consists of >98 wt.-% Fe_3O_4. The composition of the provided material, determined by XRF, is presented in Table 5.

The material contains particles with sizes suitable for fluidized bed conversion. The bulk density of MAF was measured as 2.585 g/cm^3. No evaluation of MAF as an oxygen carrier has been reported in the scientific literature before.

2.3.3. Material preparation

Before the experiments, the oxygen carriers were calcined in air in a high-temperature muffle furnace. The furnace was heated at a rate of 10 °C/min to 950 °C and the temperature was maintained for 24 h. The treatment was done to make sure the oxygen carriers were at their oxidized state at the start of the experiments. The heat treatment caused some sintering of the particles, and a mortar was used to separate them. The samples were then sieved to 125-180 μm. The resulting bulk densities were 1.42 g/cm^3 for Järnsand and 2.37 g/cm^3 for MAF.

Some oxygen carriers undergo structural and chemical changes during the first cycles of oxidation and reduction, a process often referred to as activation. The materials were activated with syngas according to Table 6, to stabilize their reactivity before the alkali addition experiments. The activation process was evaluated based on the peak CO_2 concentration during the reducing period. Around 8–10 activation cycles were done for both materials in this study, but the peak CO_2 concentration was stable already after 3–5 cycles.

2.4. Data evaluation

The fuel conversion in the experimental cycles is represented by the mass-based conversion of the oxygen carrier, ω, and the average gas yields, γ. This captures the total conversion and the distribution of C across CH_4, CO_2, and CO, the production of which results from the partial oxidation of CH_4. The mass-based conversion is defined according to Eq. (1). The final mass-based conversion for each cycle, ω_{final}, is calculated according to Eq. (2). It is assumed that the oxygen carrier is completely oxidized after the oxidation, i.e. that $\omega_{initial}$ = 100 % in all cycles.

$$\omega = \left(\frac{m}{m_{ox}}\right) \times 100\ [\%] \tag{1}$$

$$\omega_{final} = \omega_{initial} - \left(\int_{t_0}^{t_1} \frac{\dot{n} M_o}{m_{ox}} (4x_{CO_2} + 3x_{CO} - x_{H_2}) dt \right) \times 100\ [\%] \tag{2}$$

The yields of CO_2, CO, and CH_4 are calculated according to Eq. (3–6), where n is the total number of moles produced during the reduction and calculated according to Eq. (4). The yield of CH_4, γ_{CH_4}, is effectively the amount of CH_4 remaining unconverted in the outlet. When presenting the data below, it is 100-ω_{final} and the average γ for the whole cycle that are presented.

$$\gamma_{CO_2} = \frac{n_{CO_2}}{n_{CO_2} + n_{CO} + n_{CH_4}} \times 100\ [\%] \tag{3}$$

$$n_{CO_2} = \int_{t_{initial}}^{t_{final}} \dot{n} x_{CO_2} dt\ [mole] \tag{4}$$

Table 4
Elemental composition of the copper slag (Järnsand) sample material in wt.-%, provided by Boliden. Balance is mainly oxygen. The analysis method for each element is indicated.

Element	Fe[1]	Si[1]	Al[2]	Ca[1]	Mg[2]	Zn[1]	Cu[1]	Na[1]	K[2]	Mn[2]	S[1]	Ba[1]	Cr[2]	Sn[2]	Mo[2]	Ti[2]
wt.-%	35	16	2.4	2.3	1.3	1.2	0.83	0.46	0.4	0.4	0.24	0.2	0.19	0.18	0.17	0.13

[1] X-Ray Fluorescence (XRF).
[2] Flame Atomic Absorption Spectroscopy (FAAS).

Table 5
Composition of the magnetite fines (MAF) sample material in wt.-%, provided by LKAB. The elements are reported as oxides. The analysis method is X-Ray Fluorescence (XRF).

Fe_3O_4	SiO_2	K_2O	Al_2O_3	CaO	MgO	MnO	TiO_2	V_2O_5	P_2O_5
98.27	0.65	0.02	0.24	0.16	0.28	0.05	0.26	0.26	0.03

Table 6
Gas compositions and time durations for the activation cycles with diluted syngas as fuel.

Period	Gas flow (NmL/min)	Gas composition	Time
Heating	1000 NmL/min	Air in N_2 (12.4 % O_2)	
Inert	1000 NmL /min	N_2	180 s (approx.)
Start of activation cycles			
Reduction	500 NmL/min 500 NmL/min	Syngas N_2	40 s
Inert	1000 NmL /min	N_2	60 s (approx.)
Oxidation	1000 NmL/min	Air in N_2 (12.4 % O_2)	Until outlet = inlet O_2 concentration
Inert	1000 NmL /min	N_2	180 s (approx.)

$$\gamma_{CO} = \frac{n_{CO}}{n_{CO_2} + n_{CO} + n_{CH_4}} \times 100\ [\%] \quad (5)$$

$$\gamma_{CH_4} = \frac{n_{CH_4}}{n_{CO_2} + n_{CO} + n_{CH_4}} \times 100\ [\%] \quad (6)$$

Along with the gas composition, the pressure drop over the bed was also recorded throughout the whole experiment. The pressure drop is related to the fluidization of the bed. A fluidized bed compared to a defluidized bed shows a higher pressure drop and larger pressure drop fluctuations due to the formation and breakage of bubbles in the bed. The fluidization behaviour is evaluated qualitatively since it's difficult to know exactly what happens in the reactor during the experiment. Using this method has been a simple and useful way to understand how fluidization is affected throughout experiments [28,29].

2.5. Material analysis

The samples produced in the experiments were collected and analyzed with Scanning-Electron Microscopy (SEM) coupled with Energy Dispersive X-ray Spectroscopy (EDS) in a FEI ESEM Quanta 200. The back-scattering electron signal was used for the analysis and the mode used was low vacuum and 15 or 20 kV, with a working distance between 10 and 12 mm. SEM-EDS was used to map the elemental distributions in particles, to analyse the composition in points and to analyse the composition across several particles at a time. A cross-sectional surface was prepared by casting particles in an epoxy resin and then polishing them with abrasive paper. A Q150V Plus was used for sputtering a 5 nm thick gold layer on the MAF samples to avoid charging of the particles. This was not required for the Järnsand samples.

The total elemental composition was analyzed by ALS Scandinavia AB with a standard method of dissolution in $LiBO_2$- melt (ASTM D3682:2013) or HNO/HCl/HF solution (SS-EN 13656:2003) and subsequent ICP-MS (Inductively Coupled Plasma Mass Spectrometry) analysis (ISO 17294-2:2023).

2.6. Thermodynamic modelling

Thermodynamic modelling is a powerful tool for investigating the stability of chemical systems under different operating conditions. The software FactSage 8.2 was utilized to investigate the interaction between the potassium salts and the oxygen carriers Järnsand and MAF [54]. Phase diagrams were constructed using the databases FactPS and FToxid. In addition to this, the relevant compounds in the K-Fe-system $KFe_{11}O_{17}$ and $KFe_{10}O_{16}$ were included from a user-defined database [55]. The solution phases Slag-A, SpinA, MeO_A and cPyrA were considered in the calculations. Four ternary phase diagrams were generated representing different experimental conditions to evaluate the interactions and the influence of cycling between oxidizing and reducing atmospheres. Two temperatures were investigated, 850 °C and 950 °C. For each temperature, two diagrams were created, one for oxidizing and one for reducing conditions. Furthermore, as low levels of moisture influence the K-chemistry it was decided to include moisture in the calculations, that is $p(H_2O) = 0.01$ atm and 0.10 atm for oxidizing and reducing conditions, respectively.

To capture the influence of the other minor elements in Järnsand on the K-Fe-Si interactions, the Equilib-module was used to calculate the predominant phases in the material. The elemental composition of the JS_K_2CO_3_850 sample was used as input and two diagrams (at reducing and oxidizing conditions) were created. The solution phases SpinB, SlagA, cPyrA, MeO_A, Feld, Coru were considered.

3. Results and discussion

Photos of the fresh, calcined material and samples generated in the experiments are presented in Fig. 4, showing that all exposed samples contained lumps or agglomerates but in varying shapes, sizes, and amounts (the reference samples are not included and didn't have any lumps). Some colour variation can be seen, especially the MAF_K_2CO_3_950 sample is redder than the other MAF samples. This could be due to a variation in the degree of reduction. White grains of salt were present in the JS_K_2CO_3_850 and MAF_K_2CO_3_850 samples, identified in SEM-EDS analysis as K_2CO_3.

The estimated bulk densities of the samples are presented in Table 7, where the number in parenthesis shows the deviation from the density of fresh, calcined material. All Järnsand samples had a lower final density compared to the calcined Järnsand and different experimental conditions (temperature and salt addition) yielded similar results. The MAF samples showed more variation. The density of MAF_K_2CO_3_950 and MAF_KH_2PO_4_950 were 37 % and 24 % lower, respectively, than for calcined MAF, while the MAF_ KH_2PO_4_850 sample didn't change density.

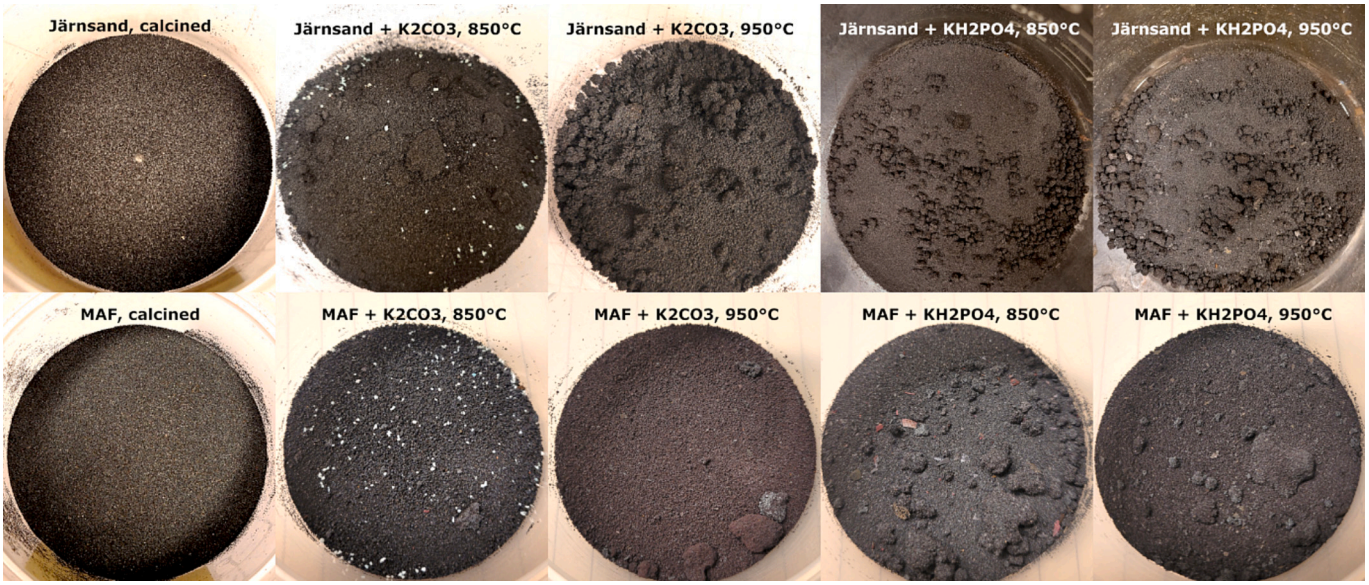

Fig. 4. Photos of the samples, exposed to 21 reduction-oxidation-cycles and K_2CO_3 or KH_2PO_4.

Table 7
Estimated bulk density (g/cm^3) of the samples after the experiments.

JS Calcined	JS_ref_850	JS_ref_950	JS_K_2CO_3_850	JS_K_2CO_3_950	JS_KH_2PO_4_850	JS_KH_2PO_4_950
1.42	1.14 (−20 %)	1.26 (−10 %)	1.16 (−18 %)	1.18 (−16 %)	1.19 (−16 %)	1.30 (−9 %)
MAF Calcined	**MAF_ref_850**	**MAF_ref_950**	**MAF_K_2CO_3_850**	**MAF_K_2CO_3_950**	**MAF_KH_2PO_4_850**	**MAF_KH_2PO_4_950**
2.37	2.52 (+6 %)	2.12 (−10 %)	1.98 (−16 %)	1.49 (−37 %)	2.22 (−1 %)	1.80 (−24 %)

Table 8 presents the measured total elemental composition of the samples. As mentioned previously, the total amount of K added in the K_2CO_3- and KH_2PO_4 experiments corresponds to 3.45 and 0.335 wt.-% of the bed, respectively, based on the initial, calcined bed material. This agrees well with the measured K-concentrations, only the MAF_K_2CO_3_950 sample had a lower K-concentration. This suggests that the added K reached the bed and was largely retained there, but there was a loss during the MAF_K_2CO_3_950 experiment, suggesting that some K exited the reactor with the flue gas during the MAF_K_2CO_3_950 experiment. The maximum theoretical K-concentrations are partly exceeded in the Järnsand experiments, which is explained by the presence of 0.4 wt.-% K in the fresh material (see Table 8).

3.1. Interactions with K_2CO_3

According to Table 8, most of the added K was retained in the sample in all experiments except for MAF_K_2CO_3_950. To understand the interaction with the oxygen carriers, it is of interest to discuss the behaviour of the model compounds when exposed to the experimental conditions. The retention of K from K_2CO_3 in the bed depends on several parameters. Previous work shows that K_2CO_3 decomposes above 900 °C into K_2O and CO_2, after which K_2O can continue to undergo other transformations [48]. A very slow decomposition in an inert atmosphere into CO_2 and K_2O, with a subsequent fast volatilization of K_2O, has been recorded also at 800 °C [47,56]. The surrounding gas phase plays an important role as the presence of CO_2 may delay decomposition [48], while the presence of steam significantly increases the release rate of K in the form of KOH (g) [56]. In the experiments, a CO_2 release was indeed recorded upon the addition of K_2CO_3, which is explained by an immediate, partial decomposition of the salt. The amount of CO_2 released depended on the experimental conditions. At 850 °C and a high K_2CO_3 addition (300 mg), the amount of CO_2 immediately released corresponded to the decomposition of around 5 % of the added salt. At 950 °C, the release corresponded to the decomposition of between 50 and 80 %. Calculating the extent of decomposition was, however, difficult since the CO_2 peak partly overlapped with the CO_2 formation

Table 8
Elemental composition (in wt.-%, balance is mainly oxygen) as determined in the total elemental analysis.

wt.-%	Fe	Si	K	P	Al	Ca	S	Cu	Mg	Mn	Na
Fresh JS*	35	16	0.4	–	2.4	2.3	0.24	0.83	1.3	0.35	0.46
JS_K_2CO_3_850	33.3	17.9	3.7	<0.1	2.7	2.1	0.3	1.0	1.0	0.3	0.5
JS_K_2CO_3_950	34.0	16.8	3.4	<0.1	2.7	1.9	0.3	1.1	1.0	0.3	0.5
JS_KH_2PO_4_850	34.4	18.7	0.8	0.3	2.7	2.0	0.3	1.0	1.0	0.3	0.6
JS_KH_2PO_4_950	35.9	17.6	0.9	0.4	2.6	2.0	0.3	1.3	0.9	0.3	0.6
Fresh MAF*	71	0.3	0.02	0.01	0.2	0.1	–	–	0.2	0.04	–
MAF_K_2CO_3_850	83.8	0.5	3.4	<0.1	0.1	0.1	<0.1	<0.1	0.1	<0.1	<0.1
MAF_K_2CO_3_950	78.9	0.5	2.0	<0.1	0.2	0.1	<0.1	0.1	0.1	<0.1	<0.1
MAF_KH_2PO_4_850	77.6	0.5	0.5	0.3	0.1	0.1	<0.1	1.6	<0.1	<0.1	<0.1
MAF_KH_2PO_4_950	86	0.5	0.4	0.3	0.1	0.1	<0.1	<0.1	0.1	<0.1	<0.1
error margin (rel)	±16 %	±13 %	±12 %	±20 %	±14 %	±13 %	±14 %	±18 %	±14 %	±13 %	±15

* according to material analysis on the fresh material, see Table 4 and Table 5. The composition of MAF has been recalculated from oxides. - = no data.

from fuel conversion. It was anyway concluded that the salt decomposed to a larger extent at a higher temperature, which agrees with the literature [47,48]. Molecular K_2CO_3 is not expected to exist in the gas phase.

3.1.1. Interactions between Järnsand and K_2CO_3

The cycling between oxidizing and reducing conditions was done to track changes in fluidization or fuel conversion. As an example, the gas concentrations of CH_4, CO_2, CO, and O_2 recorded during two separate cycles in the JS_K_2CO_3_950 experiment are presented in Fig. 5. The left graph shows data from the 9th cycle, and the right graph shows the 11th cycle. The latter shows higher CO concentrations, lower CO_2 concentrations, and a slower re-oxidation, based on the shape of the O_2-curve.

From the gas concentrations, the final mass-based conversion and gas yields, as defined in 2.4 Data evaluation, were calculated. The results of the experiments with Järnsand and the addition of K_2CO_3 are presented in Fig. 6. The left and right figure shows data for JS_K_2CO_3_850 and JS_K_2CO_3_950, respectively. The salt addition as accumulated weight is presented below the conversion graphs, and the lower graph shows the pressure drop signal during the whole experiment. The addition of K_2CO_3 started at the beginning of cycle 6. Note that the pressure drop signal and the conversion graphs are not perfectly time-synchronized due to some variations in the cycle lengths.

The methane yield (averaged over the reducing periods) was around 75 % or 55 %, depending on the experiment temperature. This methane conversion is in line with what is expected with iron-based oxygen carriers under the current conditions. The fuel conversion was relatively stable throughout the experiments, apart from a slight increase in fuel conversion during the initial 4–5 cycles. In a reference experiment without salt addition (not presented here), a similar initial increase but otherwise stable fuel conversion was observed. Between cycle 11 and 17 of the JS_K_2CO_3_950 experiment, slight variations in CO_2 and CO yields were observed, but the effect was temporary. It was also observed that the pressure drop behaviour changed drastically during the reduction in the 11th cycle, which is indicated in Fig. 6: the pressure drop and the pressure drop signal fluctuations decreased suddenly. The same change in pressure drop behaviour was observed in the JS_K_2CO_3_850 experiment at cycle 16. This type of change in the pressure drop signal suggests a defluidization of the bed, since a channelling of the gas through the bed gives rise to a lower pressure drop and lower pressure drop fluctuations, as compared to a bubbling fluidized bed. Agglomerates up to around 5 mm in size were found in the JS_K_2CO_3_950 sample, likely being the cause for defluidization since their presence enabled the formation of gas channels through the bed. The agglomerates in the JS_K_2CO_3_850 sample were softer and more irregular in size.

Two cross-section SEM micrographs of particles from the JS_K_2CO_3_950 sample are presented in Fig. 7. The left-hand image shows separate, distinct particles looking morphologically similar to the fresh material, referred to as (1) non-agglomerated. The right image shows (2) agglomerates, showing fused bed material matter with no clear particle integrity. The right image also shows many large, round cavities, suggesting the formation of gas pockets inside the material. The deformed shape of the material and the presence of cavities in the agglomerates suggest that the material has been soft and partly liquid. Similar observations have been made before, in a study where synthetic Fe_2O_3-SiO_2 combination oxygen carriers reacted with K_2CO_3 or KCl in a fixed bed [57]. The elemental compositions across the respective images are presented in Fig. 7. The average compositions across the images were obtained with SEM-EDS and is presented in at.-% on an oxygen-free basis. The average K-content in the left image (1) was 4 at.-%, with a K:Si molar ratio of 0.08. The right image (2) had more than twice as much K; around 10 at.-%, and a K:Si-rato 0.25. As a comparison, according to the total elemental analysis, the K:Si molar ratio in the sample was 0.15. The significantly higher K-content in the right image suggests that the agglomeration and change in morphology were due to an interaction with the added salt.

The elemental distributions of Fe, K, Si, Ca, and Al in some agglomerated material (in cross-section) formed in the JS_K_2CO_3_950 experiment are presented in Fig. 8. The location of K coincides with the locations of Si and Al. The surface (towards the gas phase) is enriched with Ca. The Fe is distributed as clusters or veins in the material and is largely separated from the Si, K, and Al.

Some inclusion of K was also observed in the particles that were not agglomerated. Cross-section elemental distribution maps of a particle from the JS_K_2CO_3_950 seemingly not participating in agglomeration are presented in Fig. 9. The analysis shows an Fe oxide layer on the particle surface and a depletion of Fe directly underneath. The Fe concentration in the rest of the particle was homogenous.

Iron oxide accumulation on the surface is in line with previous experiments studying the oxidation of fayalite (Fe_2SiO_4) and was seen in the initial calcination of Järnsand in this study. Mackwell [58] saw the oxidation of fayalite by the transportation of Fe-ions towards the gas-solid interface. A similar development is a well-established phenomenon for ilmenite, which separates into titanate and iron oxide during oxidation and activation [29,59]. At the studied conditions, the separation of Fe and Si is thermodynamically favoured over the formation of Fe_2SiO_4 [18].

Another observation for the Järnsand samples was the formation of a Ca-layer. Both reference and K-addition experiments showed the migration of Ca, mainly to an area right underneath the Fe-rich scales on the surface. Some Ca was also present underneath this distinct layer, but the core was depleted. K was present deep in the interior of the particle. There was a clear border dividing the K- and Ca-distribution and very little overlap between them. To investigate the surface layers further, the concentrations of Si, Fe, Ca, and K were measured in 24 evenly distributed points in a line across the layer. The location of the line and the concentrations are presented in Fig. 10. The concentration is in at.-% and on an oxygen-free basis. The graph shows clearly both the Fe-rich outer layer and the Ca-rich layer underneath, as well as an increase in

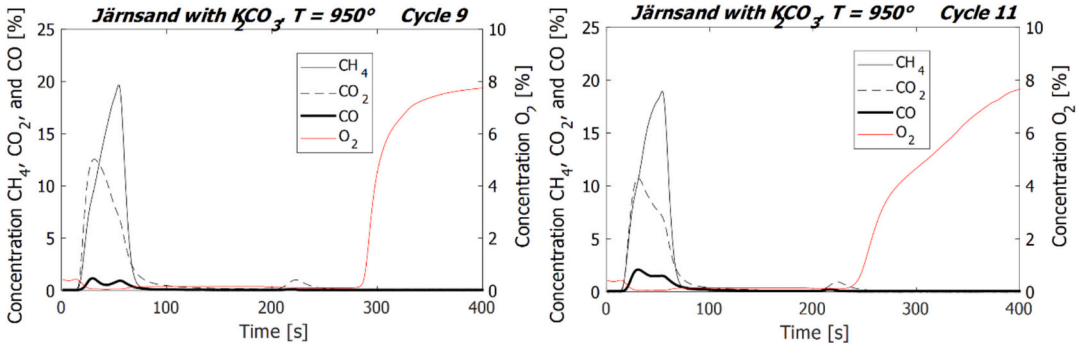

Fig. 5. Gas concentrations (CH_4, CO_2, CO, and O_2) recorded during two cycles in the JS_K_2CO_3_950 experiment. The 9th and the 11th cycles are presented, showing differences in fuel conversion and oxidation rate, attributed to the higher total addition of K_2CO_3 in cycle 11 (240 mg in 11 vs. 120 mg in cycle 9).

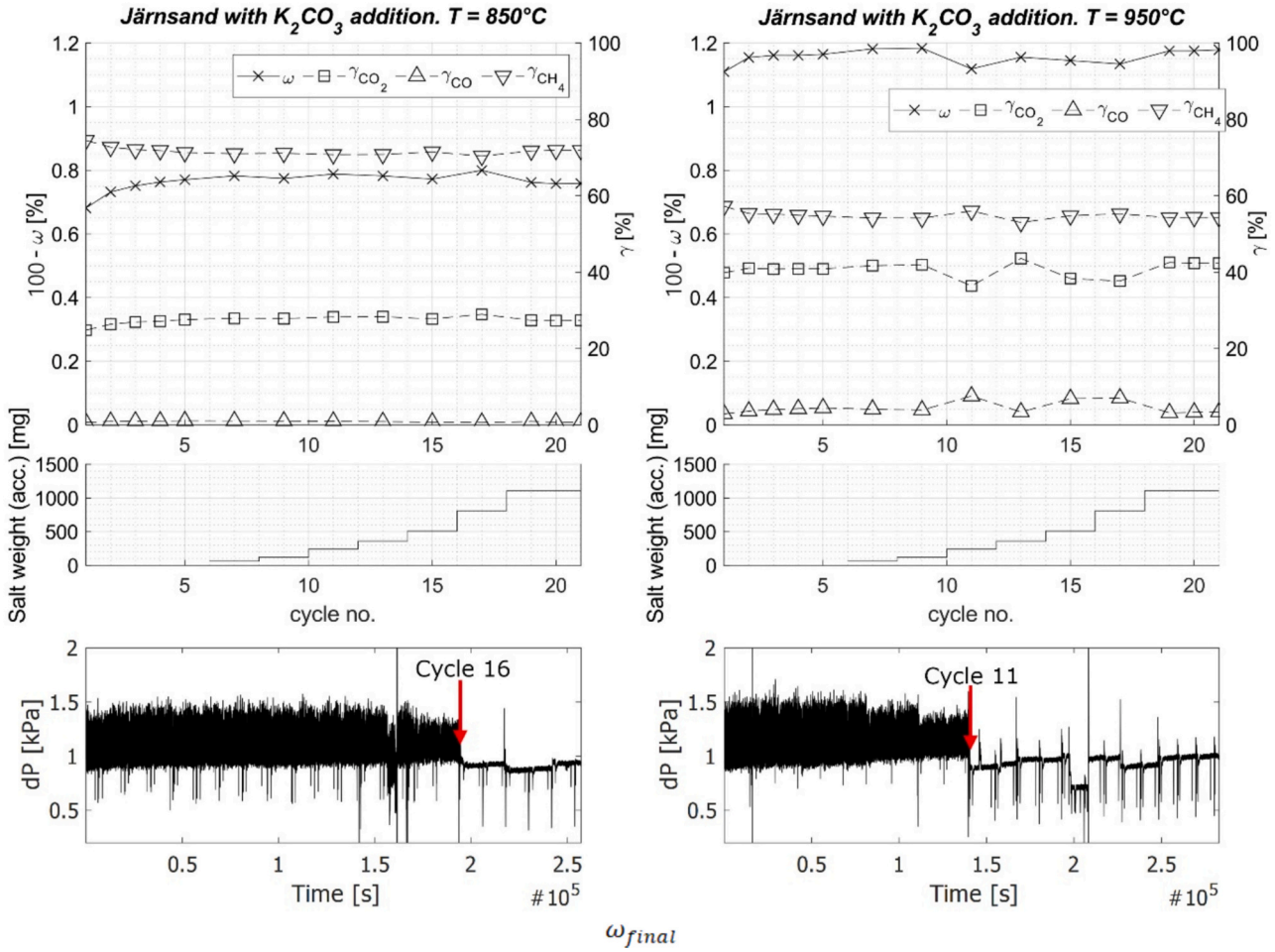

Fig. 6. Top: Mass-based conversion (ω_{final}), and CO_2-, CO-, and CH_4-yield in reduction-oxidation-cycles. Middle: The accumulated amount of salt. Lower: The pressure drop during the experiment. Left: JS_K_2CO_3_850, right: JS_ K_2CO_3_950.

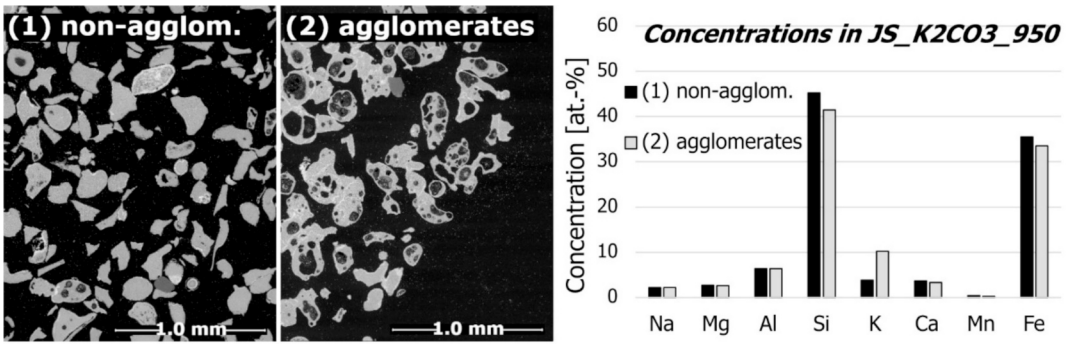

Fig. 7. SEM micrographs of particles from the JS_K_2CO_3_950 sample. The graph shows the elemental composition (in at.-%, on an oxygen-free basis) obtained from SEM-EDS analysis.

K with depth until reaching about 2.5–3 at.-% K.

Ca-layers on bed particles have been observed before in boiler samples, but a deposition mechanism rather than a migration mechanism has been suggested [59,60]. In the current study, no external Ca is added, so the layer formation must be through outwards migration. He et al. [60] studied the development of quartz bed material particles during FBC of wood-derived fuels. They found that with time, as more ash-Ca deposited on the bed particles, the melting point of the coating ash layers increased and accordingly, the amount of melt decreased. The inherent Ca-content and Ca-migration could thus potentially contribute to an agglomeration resistance of Järnsand.

In the JS_K_2CO_3_850 sample, there was no clear difference in elemental distribution between the agglomerated and the non-agglomerated particles. The elemental distribution and K:Si ratio were similar to the particles in Fig. 9. In a similar way as with the samples reacted at the higher temperature, there was also a clustering of iron towards the surface for samples exposed at 850 °C. The Fe-rich scales on the surface acted as a bridge between the agglomerated particles. Purnomo et al. [18] have previously seen agglomeration at high reduction degrees, where the bridge consists of Fe-oxide.

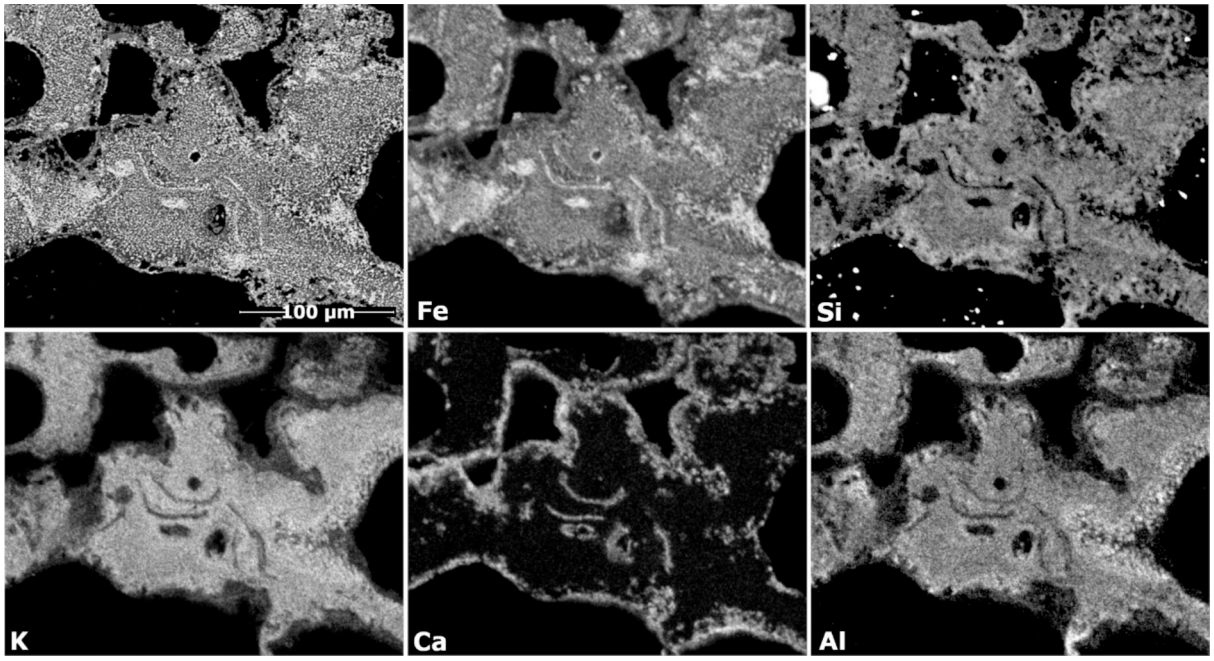

Fig. 8. SEM-EDS elemental maps of Fe, K, Si, Ca and Al in the cross-section of some agglomerated particles in the JS_K_2CO_3_950 sample.

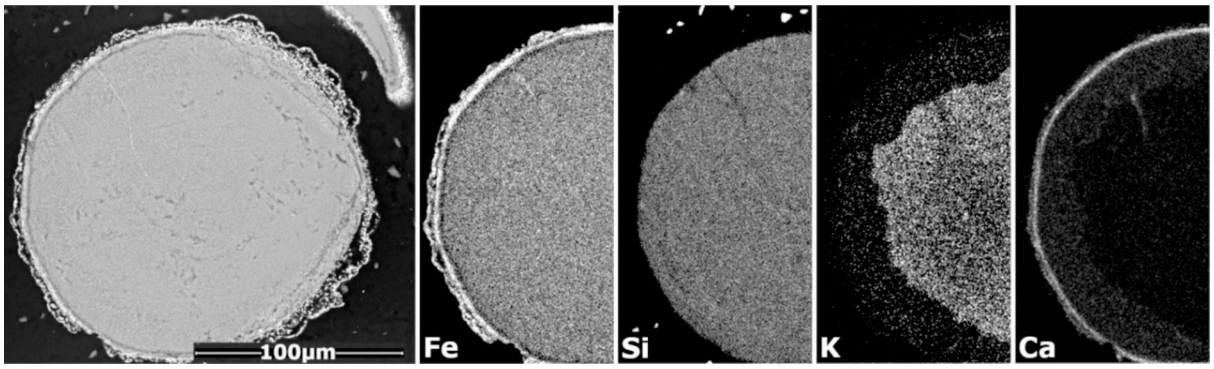

Fig. 9. SEM-EDS elemental maps of Fe, Si, K, and Ca in the cross-section of a particle from the JS_K_2CO_3_950 experiment.

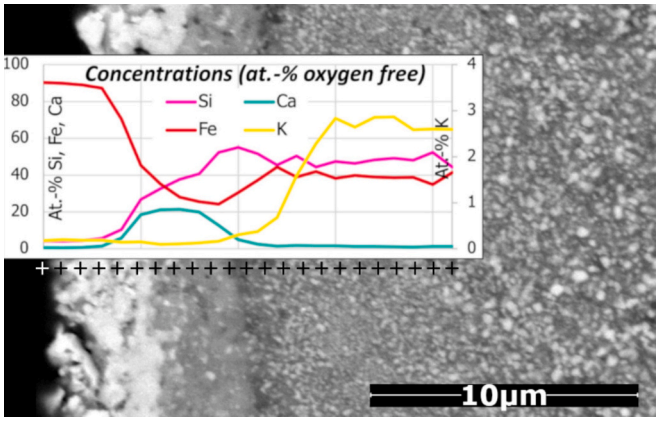

Fig. 10. Line scan analysis through the surface of a JS_K_2CO_3_950 particle not participating in agglomeration. Note that the K-concentrations are presented on the right axis.

3.1.2. *Interactions between MAF and K_2CO_3*

The fuel conversion data from the MAF_K_2CO_3_850 and MAF_K_2CO_3_950 experiments are presented in Fig. 11. The fuel conversion was not affected in the MAF_K_2CO_3_850 experiment, but the fluidization was. The disturbance started already at cycle 10, or with the addition of in total 240 mg K_2CO_3, in the end of or after the reducing period. Small, irregularly shaped agglomerates were found in the sample. A micrograph of agglomerated material is presented to the left in Fig. 12, showing porous outer layers that have fused.

In MAF_ K_2CO_3_950, on the other hand, there was a sudden increase in fuel conversion during the addition of K_2CO_3. The CO yield dropped to zero when K_2CO_3 was first introduced. Simultaneously, the CO_2 yield and ω increased while the yield of CH_4 decreased. This change happened continuously until around cycles 17–18 when the parameters stabilized. A final ω value of 1.2 wt% was reached. This was not the case for the reference experiment, where the fuel conversion was stable throughout the experiment.

The effect on the fluidization was small and the sample was mainly free from agglomerates. The few agglomerates that did form were porous in structure, as those seen to the right in Fig. 12. Neither the 950 nor the 850 °C sample agglomerates showed any sign of a melt formation, but the agglomeration was rather through sintering. The reference MAF experiments showed no defluidization or formation of

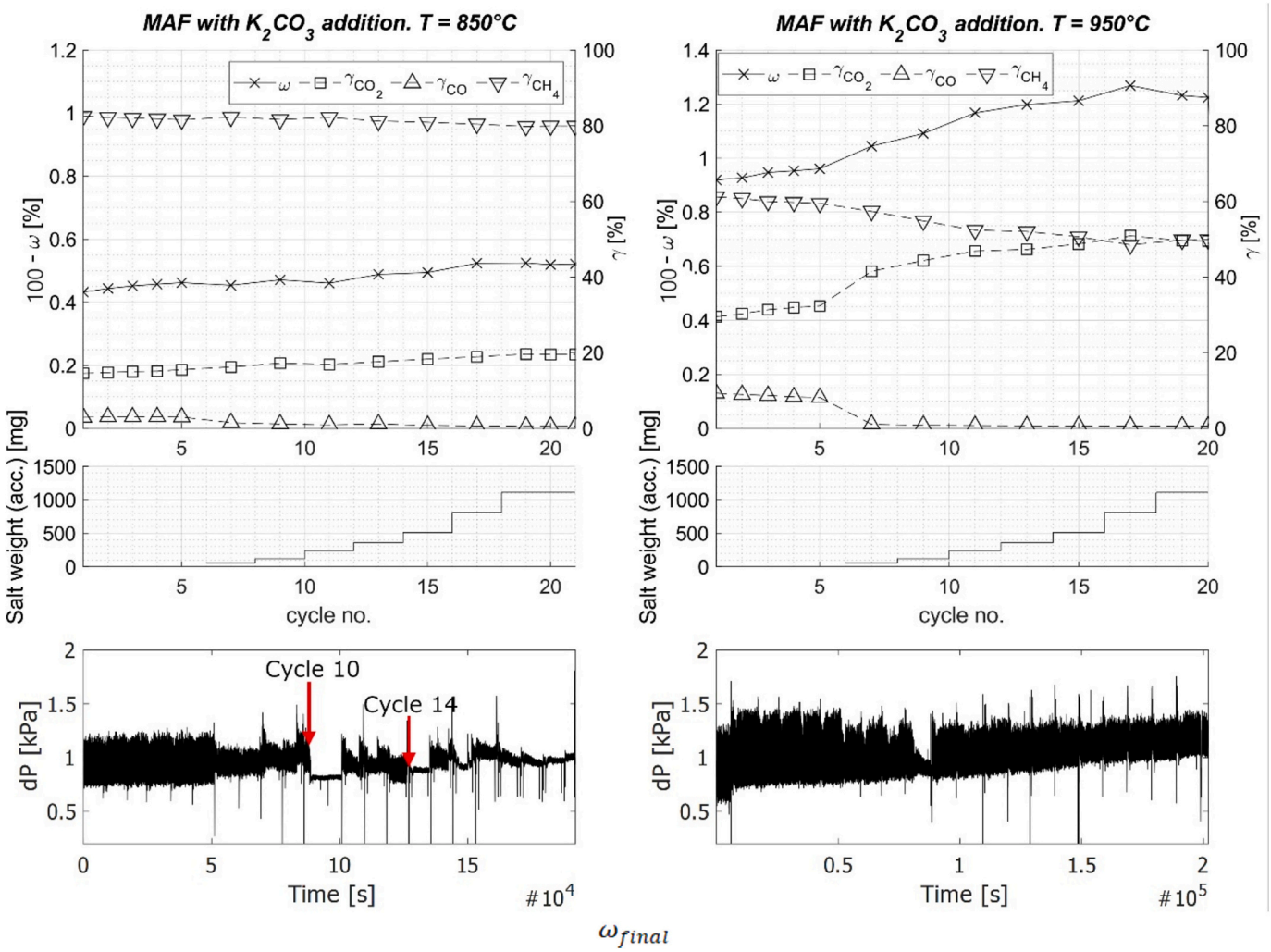

Fig. 11. Top: Mass-based conversion (ω_{final}), and CO_2-, CO-, and CH_4-yield in reduction-oxidation-cycles. Middle: The accumulated amount of salt. Lower: The pressure drop during the experiments. Left: MAF_K_2CO_3_850, right: MAF_K_2CO_3_950.

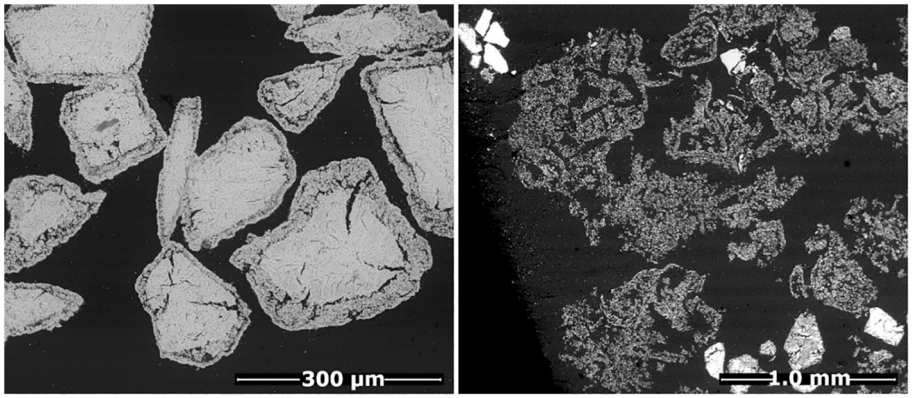

Fig. 12. SEM micrograph of agglomerates (in cross-section) (left): MAF_K_2CO_3_850 (right): MAF_K_2CO_3_950.

agglomerates, thus the agglomeration must be related to the addition of K. Interestingly, it was not found in the SEM-EDS analysis that the agglomerates like those seen in Fig. 12 should be related to a significantly higher K-concentration than the rest of the material. Possibly, the differences were not distinguishable with the current analysis method.

In general, the SEM-EDS analysis showed a low absorption of K into the MAF particles. However, structural changes in the particles were clearly promoted by K_2CO_3, which resulted in changes in density and particle morphology. The SEM-EDS analysis suggested that particles with higher porosity were correlated with a slight enrichment in K, as seen in Fig. 13. A similar effect of K_2CO_3 addition has previously been observed in iron mill scale, a material with a similar elemental composition as MAF [35]. The interactions between the iron mill scale and K_2CO_3 in a fixed bed resulted in a faster reduction of the material and a

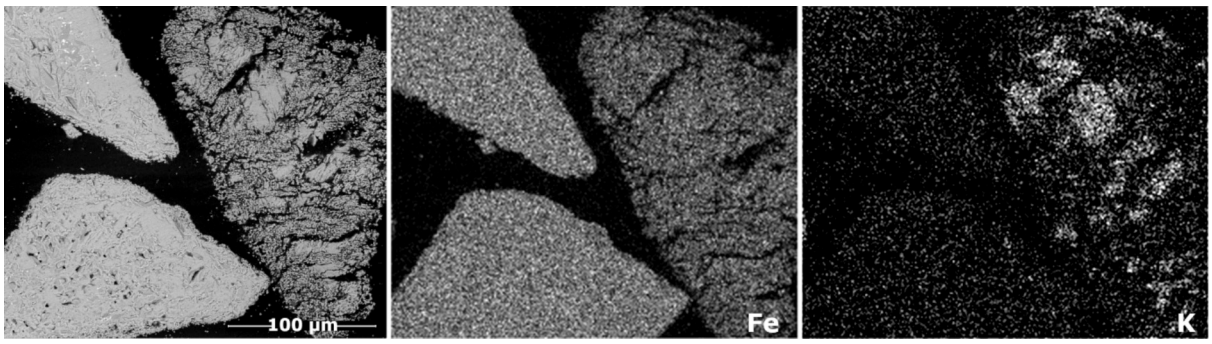

Fig. 13. SEM-EDS elemental maps of Fe and K in the cross-section of three particles from the MAF_K_2CO_3_850 sample. The particle to the right has a more porous morphology and a higher K-content, according to the analysis.

potentially more porous material. Increased porosity from interactions with K has also been demonstrated in ilmenite by Bao et al. [61] and suggested by Yang et al. [62]. They concluded that K^+ and Na^+-ions diffused into the core and that vacancies diffused in the opposite direction to neutralize the charge, resulting in the formation of pores. The development of pores with repeated oxidation and reduction has been observed also in the absence of K in oxide scales [63], as simply transitioning between different oxidation states changes the crystalline structure. However, the results from this study quite clearly show that the effect is enhanced by the addition of K. Initially, the presence of K in the MAF_K_2CO_3_950 seems to have mainly a positive effect, since the fuel conversion increased drastically. The assumed increased porosity

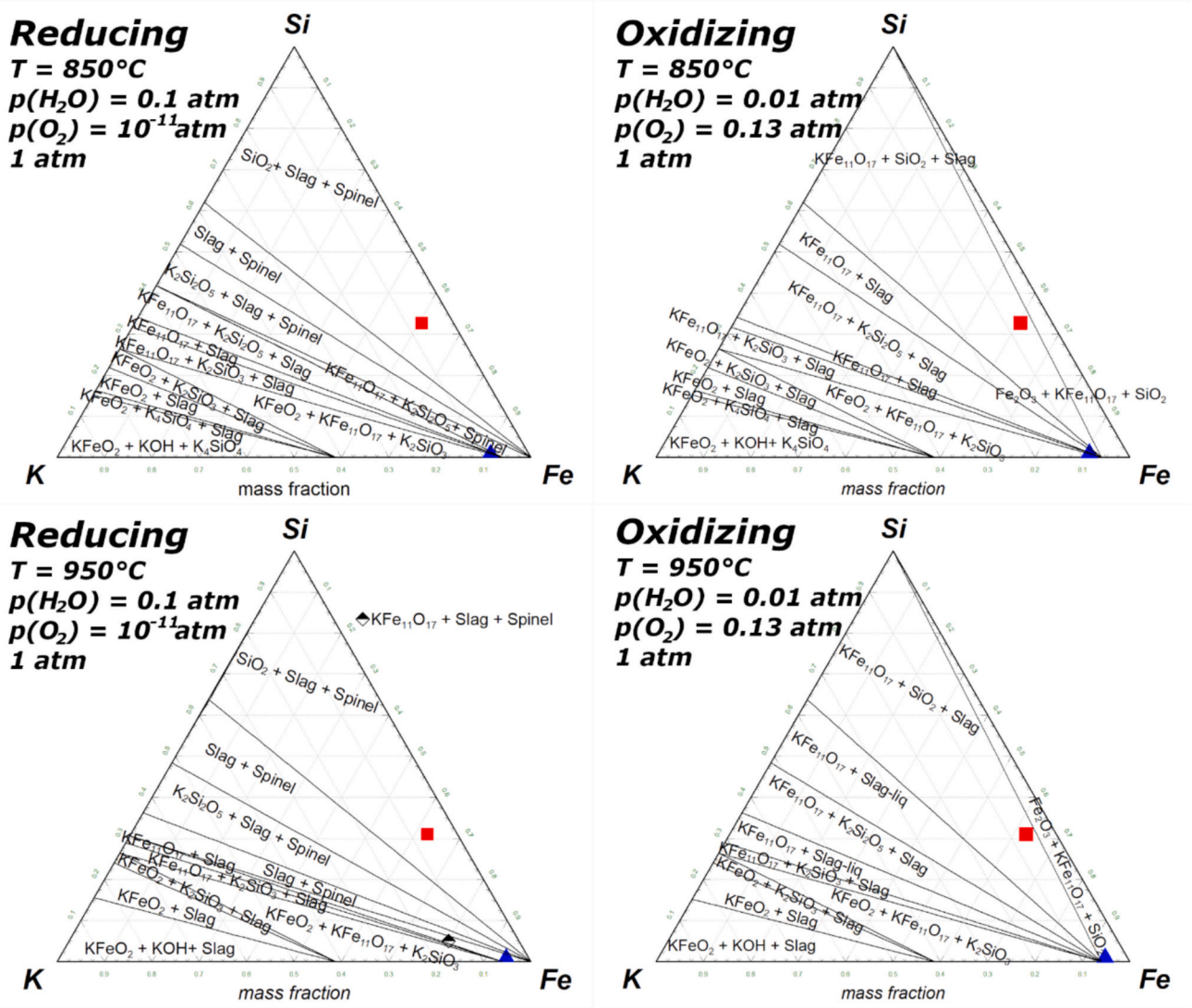

Fig. 14. Ternary phase diagrams of the Fe-Si-K system at four different conditions: a) 850 °C and reducing b) 850 °C and oxidizing, c) 950 °C and reducing, and d) 950 °C and oxidizing. The calculations were done in FactSage 8.2 Phase diagram-module.

and particle surface area have a two-fold effect on the fuel conversion (i) the solid-gas contact between oxygen carrier and fuel is enhanced (ii) the solid-gas contact between oxygen carrier and oxygen is enhanced, resulting in potentially a faster oxidation and higher final oxidation degree. However, the material also seems to have poor particle integrity in the presence of K. This potentially makes MAF unsuitable as an oxygen carrier for K-rich fuels.

3.1.3. Interactions within the K-Fe-Si system

To further understand the chemical transformations occurring in the fluidized bed, phase diagrams were constructed for the ternary system K-Fe-Si under oxidizing and reducing conditions. These phase diagrams are presented in Fig. 14. The elemental compositions of the samples are represented. The red squares show the composition of the Järnsand (JS_K_2CO_3_850 and JS_K_2CO_3_950) and the blue triangles show the composition of the MAF (MAF_K_2CO_3_850 and MAF_K_2CO_3_950) samples.

As reported before [18,58] the fayalite phase is not stable during these conditions, but Fe and Si rather separate into different phases. The ternary phase diagrams reveal that under reducing conditions, potassium is more likely to interact with silicon than with iron, leading to the formation of a melt. This melt contains K_2O, SiO_2, and, depending on the condition, also minor amounts of Fe_2O_3, $KFeO_2$, and FeO. As shown in Fig. 8, K and Si are found to coexist in the agglomerates, which aligns well with the results for Järnsand (red square) in the phase diagrams. As was also observed in the SEM/EDS analysis of JS_K_2CO_3_950, the composition differed with location in the sample, with the agglomerates showing much higher K-concentrations than the non-agglomerated particles. This shifts the location of the agglomerates towards the K-corner of the ternary diagram, and potentially, all the existing Si would exist in the form of melt in the agglomerates. Under oxidizing conditions, the slag remains, but there is also a possibility for the formation of $KFe_{11}O_{17}$. At high concentrations of Fe, this compound becomes the primary interaction path for K.

Due to relatively high concentrations of mainly Mg, Al, and Ca in Järnsand, it is of interest to also include these components when calculating the thermodynamically stable phases as this enables the binding of K in other phases. Using the composition of JS_K_2CO_3_850 as input, the predicted stable phases as a function of temperature are presented in Fig. 15 for oxidizing and reducing conditions.

At lower temperatures, feldspar (Feld, mainly $KAlSi_3O_8$ but also $NaAlSi_3O_8$ and $NaFeSi_3O_8$) is the predominant phase for K (and the Na originating from the material). Small amounts of K_2MgSiO_4 are predicted. Fe exists mainly as Fe_2O_3 (CORU) or Fe_3O_4 (SPINB) in oxidizing and reducing conditions, respectively. Si is mainly SiO_2 with a phase transition at around 860 °C. The remaining Si, Mg, Ca, and Fe exist as clinopyroxene (cPyrA, $CaFeSi_2O_6$, $CaMgSi_2O_6$, etc). At higher temperatures, the formation of a slag phase (i.e. a molten phase) is predicted, consuming the free SiO_2 and feldspar. This predicted slag phase contains mainly SiO_2 and $KAlO_2$ and minor amounts of K_2O and K_2MgSiO_4. The initial slag (melt) formation temperature is higher at oxidizing conditions (930 °C) compared to reducing conditions (905 °C).

Previous studies state that with silica sand bed material, $K_2Si_4O_9$ is likely to form when K is introduced [32], which has a melting temperature of 771 °C. The calculations presented here conclude that the presence of mainly Al, Mg, and Ca affect the K interactions in such a way that the conditions for slag formation changes, as summarized in Table 9. Minor elements present in Järnsand enables the capture of K in stable K-silicates, such as feldspar and olivine, that have higher melting temperatures than pure K-silicates [32]. Hence, the slag that is predicted for the ternary system at 850 °C is not present when taking the minor elements into account. These predictions align well with the findings in SEM-EDS, since melt was found in JS_K_2CO_3_950 but not in JS_K_2CO_3_850. This further suggests that Järnsand has a lower risk of agglomeration than silica sand in FBC of K-rich fuels. The ability of Mg and Al to protect bed material particles from sintering by forming stable K-phases such as $KAlSi_3O_8$ and $K_2MgSi_5O_{12}$ has been shown before [26,34,64]. The formation of $KAlSi_3O_8$ and $KAlSiO_4$ has also been observed in a study of interactions between potassium and red mud, which is an Fe-based oxygen carrier rich in Al and Si [41].

The formation of a melt could not be identified in the 850 °C experiment. The reasons for this could be that the compounds that form have a melting temperature above 850 °C (as suggested by the thermodynamic calculations), or that the absorption of K is too low to form enough melt for agglomeration. As was discussed previously, the release of K to the gas phase (i.e. the availability of K in a reactive form) depends on the experimental conditions and should be promoted at a higher temperature. Further, since the CH_4 conversion was higher at 950 °C, the gas surrounding the particles contained more steam, which was able

Table 9
Summary of predominant phases identified in the thermodynamic modelling.

Sample	Ternary K-Fe-Si	Equilib
JS_K_2CO_3_850	Slag (K_2O, $KFeO_2$) $KFe_{11}O_{17}$	$KAlSi_3O_8$, $KFe_{11}O_{17}$, K_2MgSiO_4
JS_K_2CO_3_950	Slag (K_2O, $KFeO_2$,) $KFe_{11}O_{17}$	Slag ($KAlO_2$, K_2O, K_2MgSiO_4) $KAlSi_3O_8$
MAF_K_2CO_3_850	$KFe_{11}O_{17}$, $K_2Si_2O_5$,	n.a.
MAF_K_2CO_3_950	Slag (K_2O)	n.a.

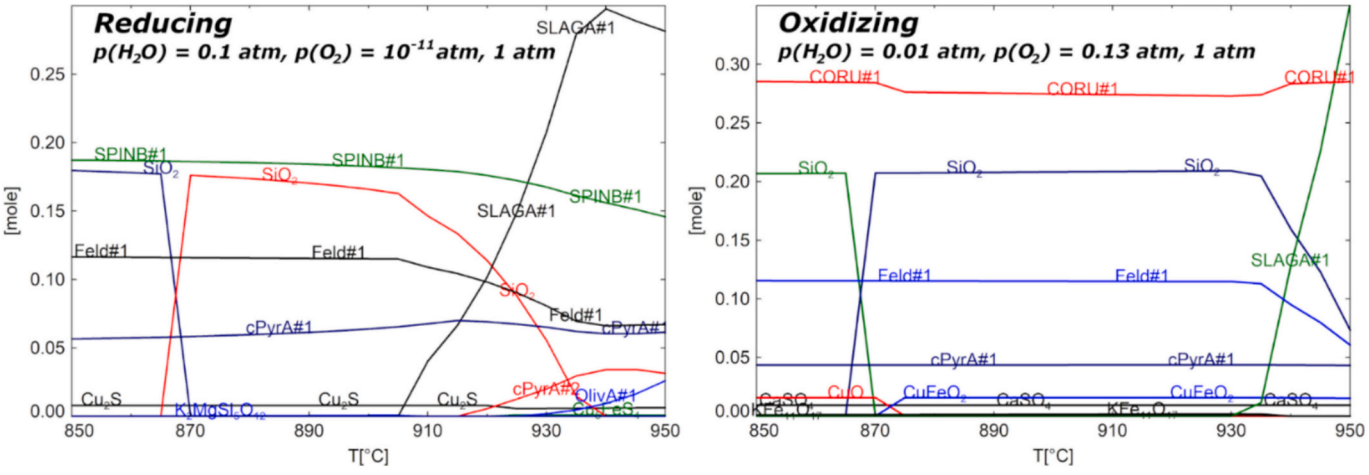

Fig. 15. Thermodynamic prediction of predominant phases between 850 and 950 °C, based on the composition of JS_K_2CO_3_850. Left: reducing conditions, right: oxidizing conditions. The calculations were done in FactSage 8.2 Equilib-module.

to enhance decomposition. At 850 °C, on the other hand, grains of K_2CO_3 were detected in the samples after the experiments, indicating that the decomposition of K_2CO_3 was slow or reversible at these conditions. Note that the total elemental analysis presented in Table 8 doesn't distinguish between K that has been absorbed by the particles and K that exists as separate salt grains, thus a quantitative evaluation of K-absorption into the oxygen carrier particles is difficult.

Agglomeration took take place in the JS_K_2CO_3_850 sample, but rather than through melt formation, the agglomeration seemed to have happened through solid-state sintering of the Fe-oxide surface layer. It's possible that the K interaction enhanced the Fe migration to the particle surface, thus promoting solid-state sintering between the Fe-oxide phases. Such a material development is difficult to quantify from these experiments alone, but a solid state sintering in fluidized beds has previously been suggested to happen in ilmenite at high degrees of reduction [8] or in the presence of K_2CO_3 [28,29]. An increased iron migration from ilmenite in the presence of K_2CO_3 was also suggested by Hildor et al. [38]. Another explanation could be that the formation of $KFe_{11}O_{17}$ promotes sintering. However, the sintering happened during reducing conditions, in which $KFe_{11}O_{17}$ was not predicted to be stable according to the phase diagrams in Fig. 14.

The decomposition of the salt suggests that the interaction was induced by gaseous KOH. KOH can also be observed in the phase diagrams in Fig. 14 at high K concentrations (lower left corner). The elemental mapping of Järnsand after exposure with K_2CO_3 showed a deep penetration of potassium into the particles (Fig. 8 and Fig. 9), and all the studied particles had at least a low K concentration in the core. A similar, deep penetration of K into Järnsand was observed also at 850 °C. Migration of K as K^+-ions within the material could be possible through a solid-state diffusion, this has been observed with ilmenite [61]. It seems, however, most likely that the initial contact with the surface has been through a gaseous K-compound. Although the literature suggests that the decomposition of K_2CO_3 starts at 900 °C (or at least is very slow below 900 °C [56]), the presence of steam in the reactor due to the conversion of CH_4 might cause enough K-release to explain the interactions seen also at 850 °C.

Looking at the calculation results for MAF (the blue triangle in the ternary phase diagram in Fig. 14), the major compound is Fe_3O_4, followed by $KFe_{11}O_{17}$ and possibly the formation of $KFeO_2$. At 850 °C, the subsequent compound is $K_2Si_2O_5$, whereas at 950 °C, it is a slag containing K_2O and SiO_2. According to the phase diagrams, many phase transitions happen around the MAF sample's compositions. These transitions likely cause changes within the crystalline structure that weaken the particle integrity (a correlation was seen between K interaction and a weakened material structure, as seen in the elemental map of K in Fig. 13). The agglomeration mechanism in MAF_K_2CO_3 samples is difficult to determine from this study, but it seems to be through solid-state sintering. No formation of a slag phase could be suggested from the SEM analysis. As was discussed for Järnsand, it's possible that the presence of a Fe-K-oxide, like $KFe_{11}O_{17}$ forming on the particle surface could be responsible for the enhanced sintering as compared to the reference experiment.

Comparing the two oxygen carriers Järnsand and MAF, it is evident from both the material analysis and the thermodynamic calculations that järnsand has a more pronounced interaction with K, meaning that in a fluidized bed, the affinity of K towards forming K-Si-compounds will be preferred over K-Fe-compounds. This explains the higher K-retention in the JS_K_2CO_3_950 than the MAF_K_2CO_3_950 sample seen in the total elemental analysis presented in Table 8.

3.2. Interactions with KH_2PO_4

In all the KH_2PO_4 addition experiments, agglomeration was observed and attributed to the formation of a melt adhering to the particle and glueing them together. This was expected, as the KH_2PO_4 was expected to decompose into KPO_3, which has a melting point of 810 °C. No clear trend could be identified regarding under which condition (reducing or oxidizing) the bed defluidized.

3.2.1. Interactions between Järnsand and KH_2PO_4

The fuel conversion during the JS_KH_2PO_4_850 and JS_KH_2PO_4_950 experiments is presented in Fig. 16. The average fuel conversion at 850 °C didn't change with salt addition. The pressure drop behaviour changed with an increased addition of salt, but no obvious point of defluidization was seen. In the JS_KH_2PO_4_950 experiment, the fuel conversion changed continuously after the 7th cycle; the yield of CH_4 was quite constant, but there was a shift from CO_2 to CO production and an accompanying decrease in the final ω. The fluidization behaviour also started deviating when the addition of KH_2PO_4 started. The pressure drop then changed drastically at cycle 16, indicating that the addition of KH_2PO_4 eventually caused the bed to defluidize. The change happened during the oxidation. Fig. 4 shows that agglomerates formed in both samples. The agglomerates were round and hard and even in size (up to a few mm). The negative effect on the fuel conversion observed at 950 °C could possibly be explained by a layer development/agglomeration on the particles, which negatively affect the contact between the solid particle and the fuel gas.

SEM micrographs of JS_KH_2PO_4_950 are presented in Fig. 17, along with the oxygen-free bulk elemental composition in (1) non-agglomerated and (2) agglomerated material. The analysis confirms that the agglomeration was related to higher concentrations of K and P. The right-hand image (2) shows Individual particles that are still distinguishable but fused by a bridging material.

The elemental distributions of K, Ca, Fe, Si, and P across a few agglomerated particles from the JS_KH_2PO_4_950 experiment are presented in Fig. 18. Some of the K was absorbed into the particles underneath the melt, but most of the K was present in the bridging phase between the particles. The melt was not homogeneous but rather consisted of one phase rich in Si, K, and Fe, and one separate phase rich in P, K, Ca, and Fe. Four different compositions were found in the sample:

(1) The particle has a more or less homogenous elemental distribution, although a layer of K has diffused inwards close to the particle surface. This is referred to as “particle phase”.
(2) Bridge/slag phase rich in mainly Fe, P, K and Ca (seen in the micrograph as the darkest area). Some Na, Mg, and Si are present.
(3) Bridge/slag phase rich in mainly Si and K. The K:Si molar ratio is about 0.25. Low amounts of Al, Fe, and P are present.
(4) Small grains of almost pure Fe-oxide are located close to the particle surface (the brightest areas in the image).

The division into these four compositions was consistent for many agglomerated particles. The composition (in at.-%, on an oxygen-free basis) of (1), (2), and (3) as determined by point analysis are presented in Fig. 18.

The interaction between Järnsand and KH_2PO_4 was similar at 850 °C and 950 °C. A cross-section SEM micrograph of agglomerated particles in the 850 °C sample is presented in Fig. 19, showing particles, slag, and bright Fe-oxide grains on the surface.

As was discussed earlier, with the presence of Ca, Mg, P, and K, stable Ca/Mg-K-P species with high melting temperatures might form, which could protect the bed from agglomerating by capturing otherwise reactive K-species [43]. Among other examples discussed earlier, the formation of a high-temperature melting K-P-Ca phase was found in another study with LD-slag, which is rich in Ca [35]. In that study it was concluded that LD-slag was more resistant to agglomeration than a pure Fe-oxide material because of its Ca-content. The presence of the Ca- and Mg-rich slag phase found in this study shows that Ca and Mg from the bed material are indeed available for interactions with K and P. As seen in Fig. 18, most of the Ca had migrated from the particle to the surrounding melt. This is probably positive when it comes to agglomeration and slagging properties of the fuel. However, the positive effect depends

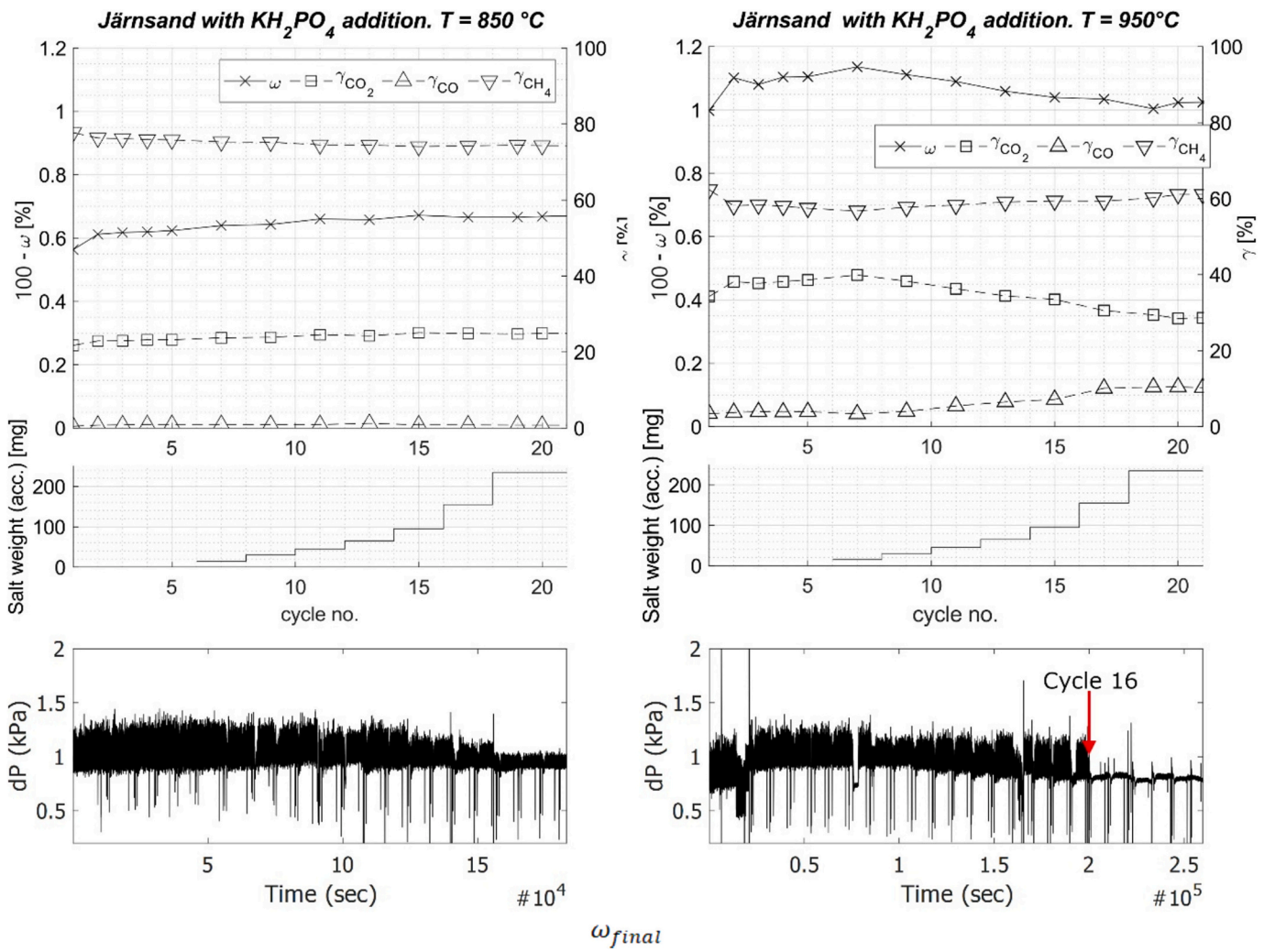

Fig. 16. Top: Mass-based conversion (ω_{final}), and CO_2-, CO-, and CH_4-yield in reduction-oxidation-cycles. Middle: The accumulated amount of salt. Lower: The pressure drop during the experiments. Left: JS_KH_2PO_4_850, right: JS_KH_2PO_4_950.

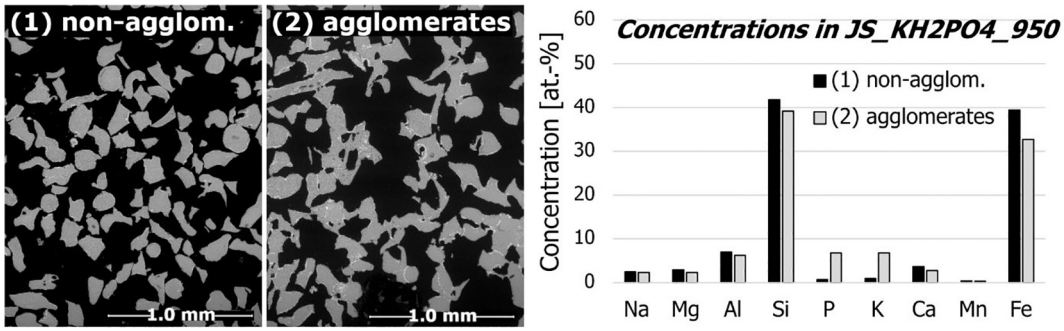

Fig. 17. Cross-section SEM micrographs of (1) non-agglomerated and (2) agglomerated material in the JS_KH_2PO_4_950 sample. The graph shows the elemental composition (at.-%, on an oxygen-free basis) obtained from SEM-EDS analysis.

on the ratios of available Mg and Ca over K and P. A larger addition of KH_2PO_4 would likely result in severe agglomeration.

3.2.2. *Interactions between MAF and KH_2PO_4*

The addition of KH_2PO_4 to MAF had no significant effect on the fuel conversion, as seen in Fig. 20. The effect on the fluidization was not conclusive: from the pressure fluctuations, the fluidization seemed to be immediately affected by KH_2PO_4 addition in the 850 °C experiment but recovered after a while. At 950 °C, the fluidization changed suddenly in cycle 14, during the reduction. The observation was that the agglomerates in the 850 °C sample were much harder and more frequent than in the 950 °C sample. The sample density decreased at 950 °C, but not as much as with K_2CO_3 (see Table 7).

The agglomerates were found to be formed by the formation of a melt, as seen in the SEM micrograph in Fig. 21 for MAF_KH_2PO_4_850. The agglomerates in the MAF_KH_2PO_4_950 sample were similar. Included in the figure are the compositions (in at.-%, on an oxygen-free basis) of (1) a dark grey, molten slag phase and (2) bright grey particles,

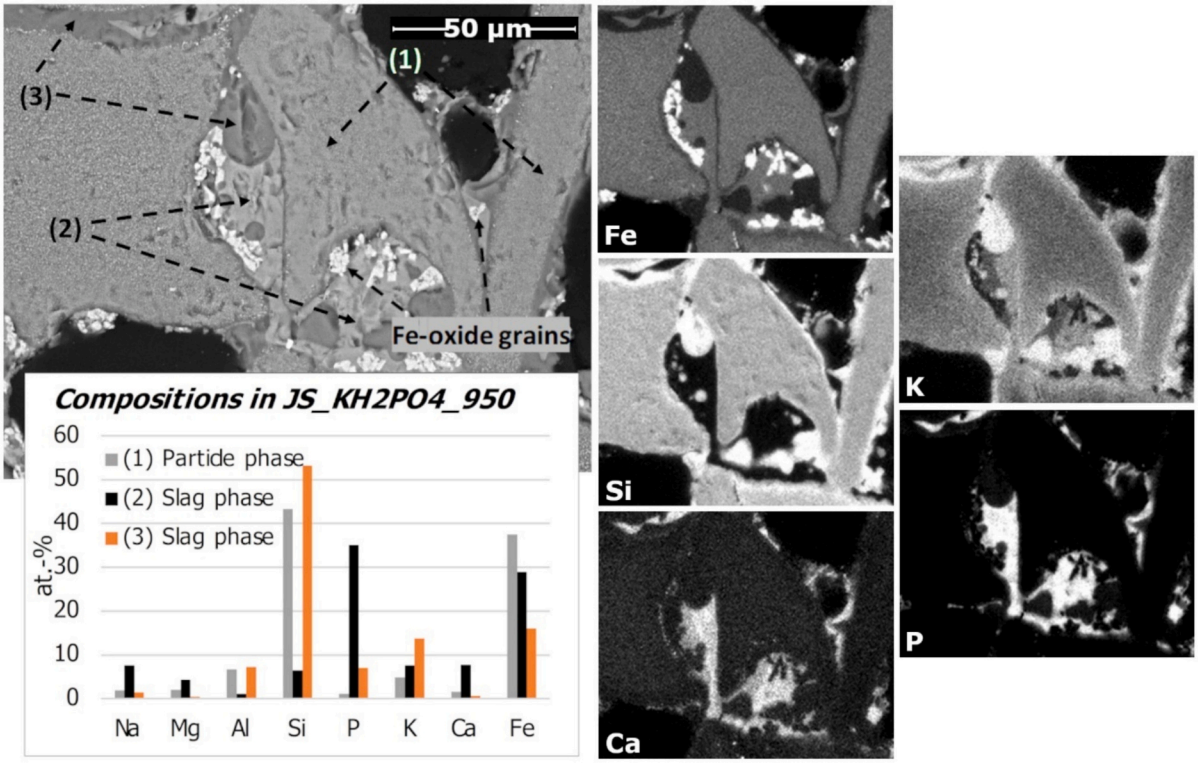

Fig. 18. SEM-EDS elemental distribution maps of Fe, K, Si, Ca, and P in the cross-section of agglomerates formed in the JS_KH_2PO_4_950 experiment. The oxygen-free elemental compositions of three distinguishable phases are presented: (1) The particle phase, where the composition resembles Järnsand (2) the P-Fe-rich slag phase with a lighter shade, and (3) the Si-K-rich slag phase that has a darker shade.

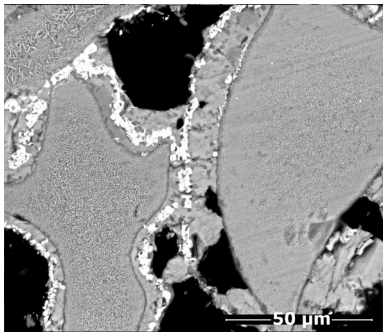

Fig. 19. SEM micrograph of the cross-section of agglomerated particles in the JS_KH_2PO_4_850 sample.

as determined by point analysis. The melt has about equal molar amounts of K, P, and Fe. Some Si was absorbed by the melt as well. The K-content inside the particles is very low. A similar melt composition has been seen previously in fixed bed interactions between KH_2PO_4 and iron mill scale [35]. Although the evaluation of the fluidization is qualitative rather than quantitative, it could be suggested that KH_2PO_4 addition affected MAF more than Järnsand. The sample photos (Fig. 4) suggest larger agglomerates in MAF. This further strengthens the hypothesis that the existence of Mg and Ca in the Järnsand is positive concerning agglomeration.

3.3. Summary of results

A summary of the experimental findings is provided in Table 10. It is evident from the above analysis that the two alkali salts interacted to various extents with the two oxygen carriers. The interactions resulted in altered fuel conversion, agglomeration, altered fluidization, and changes in the chemical compositions. It is assumed in this discussion that the formation of agglomerates is closely related to the changes observed in fluidization behaviour, although that is a simplification. The samples were extracted after the final reduction with subsequent cooling for several hours in an inert atmosphere, so what is observed in the material analysis might not represent well the morphology of the samples when they are active in the experiment. Further, from this study alone, it's not possible to present a timeline for the development of the material, since it's only observed after the experiment. However, as is seen from the material analysis, K is not evenly distributed within the samples. This allows us to say something about how the effect of K absorption differs with the concentration of K, for example, if agglomeration is related to a higher K concentration.

The interactions between Järnsand and K_2CO_3 resulted in agglomeration at both 850 °C and 950 °C, but seemingly with different mechanisms. At 950 °C, the agglomeration was related to increased K-concentrations and the presence of a melt resulting from the interaction between K and Si. Many particles in the JS_K_2CO_3_950 sample had an intact particle shape and moderate amounts of absorbed K (the K:Si molar ratio was about 0.08). Due to the presence of these low-K particles in the JS_K_2CO_3_950 sample, the material was not assumed to have become fully saturated with K. Assuming that a K:Si molar ratio of 0.25 (seen in the agglomerates) is the maximum uptake of K, the saturation limit would be something like 56 g per kg of Järnsand (or the addition of 2000 mg of K_2CO_3 in this experiment). In practice, however, the operation limit is reached when the particles become too agglomerated to operate well in a fluidized bed.

In the JS_K_2CO_3_850 and the MAF_K_2CO_3 experiments, slag/melt formation could not be concluded from the material analysis, but the agglomeration was rather through solid-state sintering of the Fe-oxides on the particle surfaces.

Material analysis results for KH_2PO_4 showed that KH_2PO_4 primarily formed a slag and limited interaction occurred with the oxygen carrier in

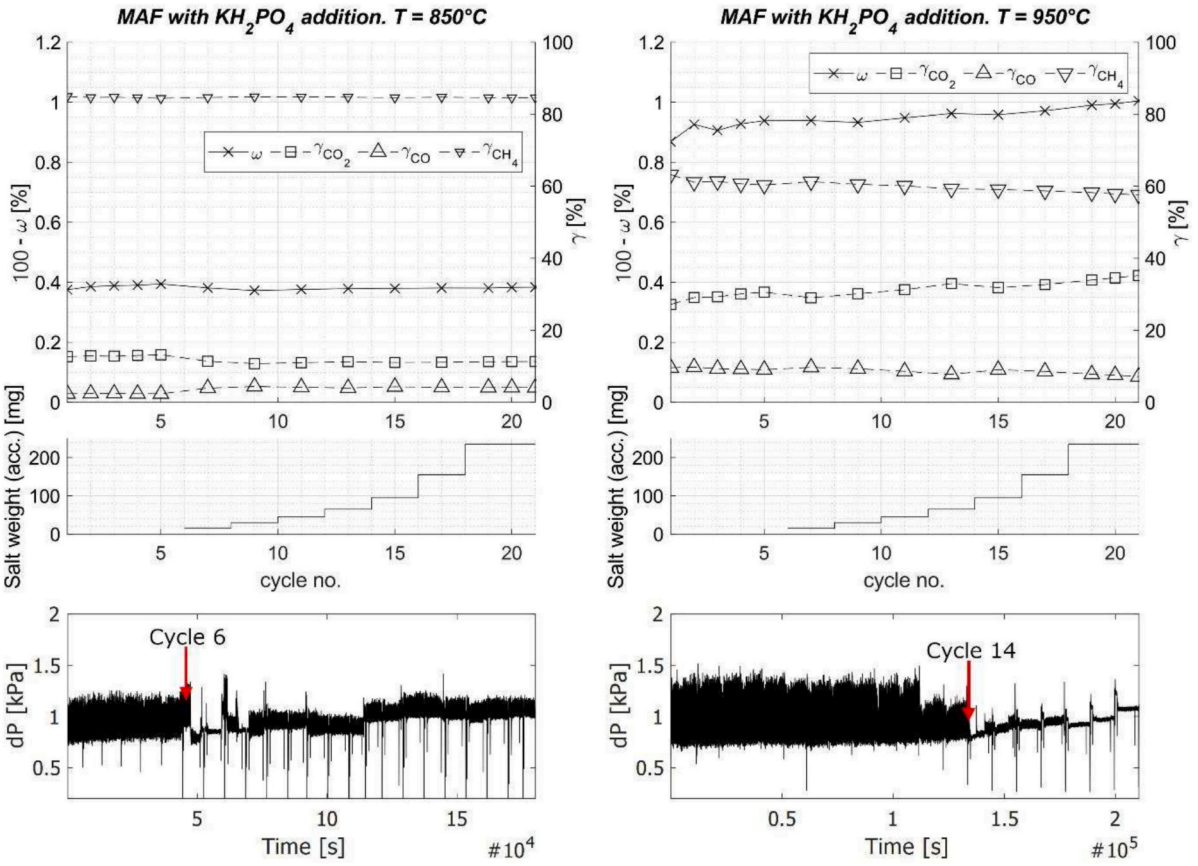

Fig. 20. Top: Mass-based conversion (ω_{final}), and CO_2-, CO-, and CH_4-yield in reduction-oxidation-cycles. Middle: The accumulated amount of salt. Lower: The pressure drop during the experiments. Left: MAF_KH_2PO_4_850, right: MAF_KH_2PO_4_950.

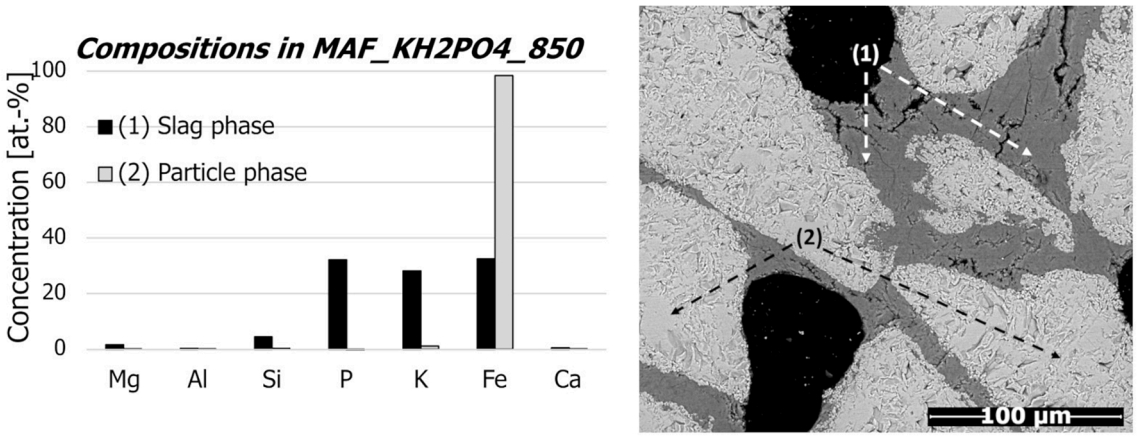

Fig. 21. SEM micrograph (right) and elemental point analysis (left) of the cross-section of agglomerates in the MAF_KH_2PO_4_850 sample.

question. In Järnsand, Ca and Mg migrated to the melt which, according to previous findings, increases the melting temperature of the K-P-phase which has a positive effect on the operation. The KH_2PO_4 cases were excluded from thermodynamic modelling studies due to clearer observations made by material analysis. Furthermore, there are limited entries in thermodynamic databases for P-bearing phases, making the calculations with P less reliable.

3.4. Practical considerations and recommendations

When it comes to practical considerations of using either MAF or Järnsand as oxygen carriers, several parameters are in play. Generally, desirable traits for bed materials include:

- Oxygen carrier effect and resistance to being de-activated (for example by being coated in ash species)
- Absorption of ash species. In this study, K and P were considered but other species are also of interest.
- Resistance to agglomeration.
- Resistance to fragmentation.
- Low cost, available in large quantities, and produced locally.
- Environmentally friendly

Both Järnsand and MAF reached a mass-based conversion of around

Table 10
Summary of the experimental findings. The K concentration is from the total elemental composition as determined by ALS Scandinavia.

Experiment	Fuel conversion	Fluidization	Visual	Cross-section SEM-EDS analysis	K (wt.-%)
JS_ref_850	Stable	Stable	No agglomerates, similar to fresh, calcined material.	Outer Fe-layer, inner Ca-layer.	n.a.
JS_ref_950	Stable	Stable	No agglomerates, similar to fresh, calcined material.	Outer Fe-layer, inner Ca-layer.	n.a.
JS_K_2CO_3_850	Stable	Defluidization with 910 mg K_2CO_3	Some agglomerates (soft, easy to break). Browner colour. White salt grains.	K in the core. Outer Fe-layer, inner Ca-layer. Agglomerates with moderate K-content, sintered by Fe-scales on the surface.	3.7
JS_K_2CO_3_950	Stable	Defluidization with 240 mg K_2CO_3	Many agglomerates in various sizes.	K in the core. Outer Fe-layer, inner Ca-layer. Agglomerates of deformed and fused particles, high K-content, and cavities.	3.4
JS_KH_2PO_4_850	Stable	Fluidization was affected	Many round agglomerates, a few mm large (hard, difficult to break).	Melt formation (Si, K, P, Ca) between particles. Low K-concentration inside the particles.	0.8
JS_KH_2PO_4_950	Decreased	Defluidization with 155 mg KH_2PO_4	Many round agglomerates, a few mm large (hard, difficult to break).	Melt formation (Si, K, P, Ca) between particles. Low K-concentration inside the particles.	0.9
MAF_ref_850	Small increase	Stable	No agglomerates, similar to calcined.		n.a.
MAF_ref_950	Small increase	Stable	No agglomerates, similar to calcined.		n.a.
MAF_K_2CO_3_850	Stable	Fluidization was affected	Very small agglomerates. White salt grains.	Some particles with porous/cracked morphology, related to increased K-concentration.	3.4
MAF_K_2CO_3_950	Large increase	Stable	A few large agglomerates (soft, easy to break). Significantly larger sample volume.	Porous/cracked morphology. Agglomerates of very porous structure, no sign of melt formation.	2.0
MAF_KH_2PO_4_850	Stable	Fluidization was affected.	Many hard agglomerates.	Melt formation (Fe, K, P) between particles. Low K-concentration inside the particles.	0.5
MAF_KH_2PO_4_950	Stable	Defluidization with 95 mg KH_2PO_4	Some agglomerates, in different sizes.	Melt formation (Fe, K, P) between particles. Low K-concentration inside particles.	0.4

1 wt.-% at 950 °C, which is considered a reasonable degree of reduction in CLC applications, as the bed material circulation will depend rather on the heat supply to the fuel reactor than the oxygen transfer [5]. In OCAC, the oxygen-carrying effect of the bed material is a complement to the conventional gas phase oxygen also present in the boiler. In that case, even a material with a lower oxygen-carrying capacity could be a suitable alternative.

Regarding the lifetime in operation, there's a trade-off between the different traits. On the one hand, absorption of K is positive for the boiler, but if absorption leads to the formation of melt, a high bed regeneration is required to limit the risk for defluidization. This is the case for Si-sand, which is anyway feasible to use as bed material because it has a low cost. In some cases, it might be advantageous to add a K-capturing agent (like bauxite or dolomite) to give the bed material a longer lifetime in the boiler. The overall risk of agglomeration for Järnsand with high-K fuels can be assumed to be lower than with conventional silica sand, and more in line with ilmenite, when compared to a previous study with ilmenite with a similar method. In the case of OCAC, the operation will likely be similar as in conventional FBC, so the expected alkali-related problems are well-known. In CLC, on the other hand, there are still unknowns regarding the process conditions and accordingly, the behaviour of the alkali. Due to the thermodynamics of the CLC process, the air reactor should be operated at a higher temperature, and ideally, the gas phase alkali should be concentrated to the fuel reactor. It is therefore of interest to understand not only how the oxygen carriers are affected by ash, but also the stability of the alkali in the oxygen carrier at oxidizing conditions. The retention of alkali in ilmenite has been investigated in previous studies [45,65], and similar studies should be conducted for Järnsand to understand the stability of the formed alkali silicate phases.

The advantages of MAF are that it is a very pure product only containing small amounts of Si and trace amounts of other metals, that it's produced at a large scale (the annual Swedish production is several millions of tons [13]) and that it shows oxygen carrier properties. The disadvantages found in this study are that MAF is a poor K-absorber and potentially has poor material integrity that could result in fragmentation, especially in the presence of K (although the current study is not suitable for determining the attrition of materials quantitatively). The current study should not, however, disqualify the utilization of MAF in other applications, such as the conversion of gaseous fuels or in related chemical-looping applications such as steam reforming. It could also be interesting to consider using MAF in combination with other oxygen carriers, or with the addition of an ash-absorbent (like dolomite).

4. Conclusions

In this work, the interactions between ash model compounds (K_2CO_3 or KH_2PO_4) and the oxygen carriers Järnsand and magnetite fines have been studied under conditions relevant to chemical-looping combustion and oxygen carrier aided combustion. Interaction experiments were conducted in a laboratory-scale fluidized bed, in which the fluidization behaviour and fuel conversion were evaluated. Samples were subsequently studied with SEM and EDS to determine any changes in morphology and elemental distribution. Thermodynamic calculations were done with the K_2CO_3 addition cases to further increase the understanding of the interactions occurring with the oxygen carriers and to investigate the influence of minor components. The KH_2PO_4 cases were excluded from the thermodynamic modelling due to clearer observations made by material analysis, where a K- and P-rich melt was identified in all cases.

The conclusions from the study are that:

- The addition of the ash model compounds had almost no effect on methane conversion, apart from the combination of MAF and K_2CO_3 at 950 °C, in which the conversion was drastically increased. This was attributed to an increased porosity and thus higher solid-gas contact as compared to the reference case.
- With Järnsand, K from K_2CO_3 interacted with the material, forming mainly K-Al-silicates and K-Mg-silicates. Slag was found at 950 °C but not at 850 °C. Thermodynamic modelling showed that the slag formation temperature was around 910–930 °C, which is higher than for pure K-silicates. At lower temperatures, solid K_2MgSiO_4 and $KAlSi_3O_8$ were the predicted K-phases, showing that the minor elements in the material are

of central importance for the alkali chemistry. With KH_2PO_4, a K-P-melt formed, and Ca was absorbed into the melt possibly also having a positive effect on the agglomeration by increasing the melting temperature of the slag. Nevertheless, agglomerates formed at both 850 and 950 °C.

- With MAF, the uptake of K was low. The material analysis and thermodynamic modelling showed that the affinity of K towards forming K-Si-compounds is preferred over forming K-Fe-compounds. The predicted K-Fe-phases were $KFe_{11}O_{17}$(s) and $KFeO_2$ (slag). With KH_2PO_4, melt formed on the surface causing agglomeration. Fe was absorbed into the K-P-melt.
- Both Järnsand and MAF reach around 1wt.-% of mass-based conversion during the fuel cycle, making them promising oxygen carriers for various chemical-looping processes as an alternative to ilmenite. However, MAF might suffer from poor particle integrity in the presence of K-rich ash species.

Author statement (Credit)

Felicia Störner: Methodology, Investigation, Formal Analysis, Visualization, Writing – Original Draft, Writing – Review & Editing.

Ivana Staničić: Investigation, Visualization, Writing – Original Draft, Writing – Review & Editing.

Pavleta Knutsson: Supervision, Writing – Review & Editing.

Tobias Mattisson: Supervision, Writing - Review & Editing.

Magnus Rydén: Conceptualization, Supervision, Writing – Review & Editing, Funding acquisition.

CRediT authorship contribution statement

Felicia Störner: Writing – review & editing, Writing – original draft, Visualization, Validation, Methodology, Investigation, Formal analysis, Data curation. **Ivana Staničić:** Writing – original draft, Validation, Methodology, Investigation, Data curation. **Pavleta Knutsson:** Writing – review & editing, Validation, Supervision, Methodology, Investigation, Conceptualization. **Tobias Mattisson:** Writing – review & editing, Supervision, Methodology, Investigation, Conceptualization. **Magnus Rydén:** Writing – review & editing, Validation, Supervision, Project administration, Methodology, Investigation, Funding acquisition, Formal analysis, Data curation, Conceptualization.

Declaration of competing interest

The authors declare that they have no known competing financial interests or personal relationships that could have appeared to influence the work reported in this paper.

Data availability

Data will be made available on request.

Acknowledgements

This research was funded by the Swedish Research Council 2017–04553, and by the Swedish Energy Agency 2022-00557. Järnsand was provided by Boliden Minerals MAF was provided by LKAB. This work was performed in part at the Chalmers Material Analysis Laboratory, CMAL.

References

[1] T. Mattisson, et al., Chemical-looping technologies using circulating fluidized bed systems: Status of development, Fuel Process. Technol. 172 (2018) 1–12, https://doi.org/10.1016/j.fuproc.2017.11.016.

[2] N.E.L. Haugen, et al., Building the world's largest Chemical Looping Combustion (CLC) unit, Int. J. Greenh. Gas Control 129 (2023) 103975, https://doi.org/10.1016/j.ijggc.2023.103975.

[3] Z. Li, T. Lei, "能动系研究团队在化学链燃烧技术研究中取得重大进展," Department of Energy and Power Engineering, Tsinghua university, 2024. Accessed: Jul. 25. [Online]. Available: https://www.te.tsinghua.edu.cn/info/1095/3291.htm.

[4] P. Ohlemüller, J. Ströhle, B. Epple, Chemical looping combustion of hard coal and torrefied biomass in a 1 MWth pilot plant, Int. J. Greenh. Gas Control 65 (2017) 149–159, https://doi.org/10.1016/j.ijggc.2017.08.013.

[5] A. Lyngfelt, D. Pallarès, C. Linderholm, F. Lind, H. Thunman, B. Leckner, Achieving Adequate Circulation in Chemical Looping Combustion—Design Proposal for a 200 MWth Chemical Looping Combustion Circulating Fluidized Bed Boiler, Energy Fuel 36 (2022) 9588–9615, https://doi.org/10.1021/acs.energyfuels.1c03615.

[6] A. Lyngfelt, B. Leckner, A 1000 MWth boiler for chemical-looping combustion of solid fuels – Discussion of design and costs, Appl. Energy 157 (2015) 475–487, https://doi.org/10.1016/j.apenergy.2015.04.057.

[7] A. Lyngfelt, A. Brink, Ø. Langørgen, T. Mattisson, M. Rydén, C. Linderholm, 11,000 h of chemical-looping combustion operation—where are we and where do we want to go? Int. J. Greenh. Gas Control 88 (2019) 38–56, https://doi.org/10.1016/j.ijggc.2019.05.023.

[8] V. Purnomo, D. Yilmaz, H. Leion, T. Mattisson, Study of defluidization of iron- and manganese-based oxygen carriers under highly reducing conditions in a lab-scale fluidized-bed batch reactor, Fuel Process. Technol. 219 (2021) 106874, https://doi.org/10.1016/j.fuproc.2021.106874.

[9] B. Leckner, Developments in fluidized bed conversion of solid fuels, Therm. Sci. 20 (2016) S1–S18, https://doi.org/10.2298/TSCI150703135L.

[10] F. Lind, A. Corcoran, B.-Å. Andersson, H. Thunman, 12,000 hours of operation with oxygen-carriers in industrially relevant scale, VGB PowerTech 7 (2017) 1–6.

[11] H. Thunman, F. Lind, C. Breitholtz, N. Berguerand, M. Seemann, Using an oxygen-carrier as bed material for combustion of biomass in a 12-MWth circulating fluidized-bed boiler, Fuel 113 (2013) 300–309, https://doi.org/10.1016/j.fuel.2013.05.073.

[12] F. Lind, A. Corcoran, H. Thunman, Validation of the oxygen buffering ability of bed materials used for OCAC in a large scale CFB boiler, Powder Technol. 316 (2017) 462–468, https://doi.org/10.1016/j.powtec.2016.12.048.

[13] F. Störner, F. Lind, M. Rydén, Oxygen carrier aided Combustion in Fluidized Bed Boilers in Sweden — Review and Future Outlook with respect to Affordable Bed Materials, Appl. Sci. 11 (17) (2021), https://doi.org/10.3390/app11177935.

[14] P. Moldenhauer, A. Corcoran, H. Thunman, F. Lind, A Scale-Up Project for Operating a 115 MWth Biomass-Fired CFB boiler with Oxygen Carriers as Bed Material, in: 5th International Conference on Chemical-Looping, Park City, Utah, USA, 2018.

[15] A. Gyllén, P. Knutsson, F. Lind, H. Thunman, Magnetic separation of ilmenite used as oxygen carrier during combustion of biomass and the effect of ash layer buildup on its activity and mechanical strength, Fuel 269 (2020) 117470, https://doi.org/10.1016/j.fuel.2020.117470.

[16] M. Rydén, M. Hanning, F. Lind, Oxygen carrier aided Combustion (OCAC) of Wood Chips in a 12 MW th Circulating Fluidized Bed Boiler using Steel Converter Slag as Bed Material, Appl. Sci. 8 (12) (2018), https://doi.org/10.3390/app8122657.

[17] F. Hildor, et al., LD slag as an oxygen carrier for combustion processes, in: 5th International Conference on Chemical Looping, Park City, Utah, USA, 2018.

[18] V. Purnomo, I. Staničić, T. Mattisson, M. Rydén, H. Leion, Performance of iron sand as an oxygen carrier at high reduction degrees and its potential use for chemical looping gasification, Fuel 339 (2023) 127310, https://doi.org/10.1016/j.fuel.2022.127310.

[19] M. Zevenhoven, P. Yrjas, M. Hupa, Handbook of Combustion, Chapter 14: Ash-Forming Matter and Ash-Related Problems vol. 4, Wiley-VCH, Weinheim, 2010.

[20] L.J.R. Nunes, J.C.O. Matias, J.P.S. Catalão, Biomass combustion systems: a review on the physical and chemical properties of the ashes, Renew. Sust. Energ. Rev. 53 (2016) 235–242, https://doi.org/10.1016/j.rser.2015.08.053.

[21] A.A. Khan, W. de Jong, P.J. Jansens, H. Spliethoff, Biomass combustion in fluidized bed boilers: potential problems and remedies, Fuel Process. Technol. 90 (1) (2009) 21–50, https://doi.org/10.1016/j.fuproc.2008.07.012.

[22] T. Berdugo Vilches, W. Weng, P. Glarborg, Z. Li, H. Thunman, M. Seemann, Shedding light on the governing mechanisms for insufficient CO and H2 burnout in the presence of potassium, chlorine and sulfur, Fuel 273 (2020) 117762, https://doi.org/10.1016/j.fuel.2020.117762.

[23] A.-L. Elled, L.-E. Åmand, B.-M. Steenari, Composition of agglomerates in fluidized bed reactors for thermochemical conversion of biomass and waste fuels Experimental data in comparison with predictions by a thermodynamic equilibrium model, Fuel 111 (1) (2013) 696–708, https://doi.org/10.1016/j.fuel.2013.03.018.

[24] E. Brus, M. Öhman, A. Nordin, Mechanisms of bed agglomeration during fluidized-bed combustion of biomass fuels, Energy Fuel 19 (3) (2005) 825–832, https://doi.org/10.1021/ef0400868.

[25] M. Kuba, N. Skoglund, M. Öhman, H. Hofbauer, A review on bed material particle layer formation and its positive influence on the performance of thermo-chemical biomass conversion in fluidized beds, Fuel 291 (2021) 120214, https://doi.org/10.1016/j.fuel.2021.120214.

[26] Y. Liu, et al., Ash chemistry in chemical looping process for biomass valorization: a review, Chem. Eng. J. 478 (2023) 147429, https://doi.org/10.1016/j.cej.2023.147429.

[27] C. Sevonius, P. Yrjas, M. Hupa, Defluidization of a quartz bed - Laboratory experiments with potassium salts, Fuel 127 (2014) 161–168, https://doi.org/10.1016/j.fuel.2013.10.047.

[28] M. Zevenhoven, et al., Defluidization of the oxygen carrier ilmenite – Laboratory experiments with potassium salts, Energy 148 (2018) 930–940, https://doi.org/10.1016/j.energy.2018.01.184.

[29] F. Störner, P. Knutsson, H. Leion, T. Mattisson, M. Rydén, An improved method for feeding ash model compounds to a bubbling fluidized bed – CLC experiments with ilmenite, methane, and K2CO3, Greenh. Gases Sci. Technol. 13 (4) (2023) 546–564, https://doi.org/10.1002/ghg.2218.
[30] D.Y. Lu, Y. Tan, M.A. Duchesne, D. McCalden, Potassium Capture by Ilmenite Ore as the Bed Material during Fluidized Bed Conversion, Fuel 335 (2023) 127008, https://doi.org/10.2139/ssrn.4232829.
[31] F. Lind, M. Israelsson, H. Thunman, Magnetic separation for the recirculation of oxygen active bed materials when combusting municipal solid waste in large scale CFB boilers, in: Clearwater clean energy conference, Florida, USA, 2018.
[32] R. Faust, T.B. Vilches, P. Malmberg, M. Seemann, P. Knutsson, Comparison of Ash Layer Formation Mechanisms on Si-Containing Bed Material during dual Fluidized Bed Gasi fi cation of Woody Biomass, Energy Fuel 34 (7) (2020) 8340–8352, https://doi.org/10.1021/acs.energyfuels.0c00509.
[33] M. Bozaghian Bäckman, A. Rebbling, M. Kuba, S.H. Larsson, N. Skoglund, Bed material performance of quartz, natural K-feldspar, and olivine in bubbling fluidized bed combustion of barley straw, Fuel 364 (2024) 130788, https://doi.org/10.1016/j.fuel.2023.130788.
[34] S. Du, H. Yang, K. Qian, X. Wang, H. Chen, Fusion and transformation properties of the inorganic components in biomass ash, Fuel 117 (2014) 1281–1287, https://doi.org/10.1016/j.fuel.2013.07.085.
[35] F. Störner, F. Hildor, H. Leion, M. Zevenhoven, L. Hupa, M. Rydén, Potassium Ash Interactions with Oxygen Carriers Steel Converter Slag and Iron Mill Scale in Chemical-Looping Combustion of Biomass - Experimental Evaluation using Model Compounds, Energy Fuel 34 (2) (2020) 2304–2314, https://doi.org/10.1021/acs.energyfuels.9b03616.
[36] D. Yilmaz, H. Leion, Interaction of Iron Oxygen Carriers and Alkaline Salts present in Biomass-Derived Ash, Energy Fuel 34 (9) (2020) 11143–11153, https://doi.org/10.1021/acs.energyfuels.0c02109.
[37] I. Staničić, J. Brorsson, A. Hellman, T. Mattisson, R. Backman, Thermodynamic Analysis on the Fate of Ash elements in Chemical Looping Combustion of Solid Fuels—Iron-based Oxygen Carriers, Energy Fuel 36 (17) (2022) 9648–9659, https://doi.org/10.1021/acs.energyfuels.2c01578.
[38] F. Hildor, M. Zevenhoven, A. Brink, L. Hupa, H. Leion, Understanding the Interaction of Potassium Salts with an Ilmenite Oxygen carrier under Dry and Wet Conditions, ACS Omega 5 (36) (2020) 22966–22977, https://doi.org/10.1021/acsomega.0c02538.
[39] I. Staničić, M. Hanning, R. Deniz, T. Mattisson, R. Backman, H. Leion, Interaction of oxygen carriers with common biomass ash components, Fuel Process. Technol. 200 (2020), https://doi.org/10.1016/j.fuproc.2019.106313.
[40] I. Staničić, V. Andersson, M. Hanning, T. Mattisson, R. Backman, H. Leion, Combined manganese oxides as oxygen carriers for biomass combustion — Ash interactions, Chem. Eng. Res. Des. 149 (2019) 104–120, https://doi.org/10.1016/j.cherd.2019.07.004.
[41] Y. Yang, Y. Shao, S. Ma, P. Li, T. Song, Biomass ash chemistry in oxygen carrier aided combustion: Interaction between potassium and red mud, Fuel 357, no. PA (2024) 129720, https://doi.org/10.1016/j.fuel.2023.129720.
[42] P. Piotrowska, et al., Fate of alkali metals and phosphorus of rapeseed cake in circulating fluidized bed boiler part 1: Cocombustion with wood, Energy Fuel 24 (1) (2010) 333–345, https://doi.org/10.1021/ef900822u.
[43] A. Grimm, N. Skoglund, D. Boström, C. Boman, M. Öhman, Influence of Phosphorus on Alkali distribution during Combustion of Logging Residues and Wheat Straw in a Bench-Scale Fluidized Bed, Energy Fuel 26 (2012) 3012–3023, https://doi.org/10.1021/ef300275e.
[44] T. Leffler, C. Brackmann, M. Berg, M. Aldén, Z. Li, Online Alkali Measurement during Oxy-fuel Combustion, Energy Procedia 120 (2017) 365–372, https://doi.org/10.1016/j.egypro.2017.07.217.
[45] I. Gogolev, A.H. Soleimanisalim, D. Mei, A. Lyngfelt, Effects of Temperature, operation Mode, and Steam Concentration on Alkali Release in Chemical Looping Conversion of Biomass - Experimental Investigation in a 10 kWth pilot, Energy Fuel 36 (2022) 9551–9570, https://doi.org/10.1021/acs.energyfuels.1c04353.
[46] V. Andersson, Y. Ge, X. Kong, J.B.C. Pettersson, A Novel Method for On-Line Characterization of Alkali Release and thermal Stability of Materials used in Thermochemical Conversion Processes, Energies 15 (12) (2022), https://doi.org/10.3390/en15124365.
[47] J.N. Knudsen, P.A. Jensen, K. Dam-Johansen, Transformation and release to the gas phase of Cl, K, and S during combustion of annual biomass, Energy Fuel 18 (5) (2004) 1385–1399, https://doi.org/10.1021/ef049944q.
[48] R.L. Lehman, J.S. Gentry, N.G. Glumac, Thermal stability of potassium carbonate near its melting point, Thermochim. Acta 316 (1) (1998) 1–9, https://doi.org/10.1016/S0040-6031(98)00289-5.
[49] H. Kassman, L. Bäfver, L.E. Åmand, The importance of SO2 and SO3 for sulphation of gaseous KCl - an experimental investigation in a biomass fired CFB boiler, Combust. Flame 157 (9) (2010) 1649–1657, https://doi.org/10.1016/j.combustflame.2010.05.012.
[50] T.K. Hannl, N. Skoglund, J. Priščák, M. Öhman, M. Kuba, Bubbling fluidized bed co-combustion and co-gasification of sewage sludge with agricultural residues with a focus on the fate of phosphorus, Fuel 357 (April) (2023) 2024, https://doi.org/10.1016/j.fuel.2023.129822.
[51] E.O. Lidman Olsson, V. Purnomo, P. Glarborg, H. Leion, K. Dam-Johansen, H. Wu, Thermal Conversion of Sodium Phytate using the Oxygen carrier Ilmenite Interaction with Na-Phosphate and its effect on Reactivity, Energy Fuel (2022), https://doi.org/10.1021/acs.energyfuels.2c00967.
[52] H. Leion, V. Frick, F. Hildor, Experimental method and setup for laboratory fluidized bed reactor testing, Energies 11 (10) (2018), https://doi.org/10.3390/en11102505.
[53] H. Leion, A. Lyngfelt, M. Johansson, E. Jerndal, T. Mattisson, The use of ilmenite as an oxygen carrier in chemical-looping combustion, Chem. Eng. Res. Des. 86 (9) (2008) 1017–1026, https://doi.org/10.1016/j.cherd.2008.03.019.
[54] C.W. Bale, et al., FactSage thermochemical software and databases, 2010-2016, CALPHAD Comput. Coupling Phase Diagrams Thermochem. 54 (2016) 35–53, https://doi.org/10.1016/j.calphad.2016.05.002.
[55] R. Faust, et al., Thermodynamic Modeling and Experimental Investigation of the System Fe−Ti−O-K for Ilmenite used as Fluidized Bed Oxygen carrier, Energy Fuel in press (2024), https://doi.org/10.1021/acs.energyfuels.4c02016.
[56] H.B. Zhao, W.T. Xu, Q. Song, J.K. Zhuo, Q. Yao, Effect of Steam and SiO2 on the Release and Transformation of K2CO3 and KCl during Biomass thermal Conversion, Energy Fuel 32 (9) (2018) 9633–9639, https://doi.org/10.1021/acs.energyfuels.8b02269.
[57] L. Chen, P. Li, T. Song, Biomass ash chemistry in chemical looping combustion: Interaction mechanism of potassium-ash and iron-based oxygen carriers, Biomass Bioenergy 183 (2024) 107154, https://doi.org/10.1016/j.biombioe.2024.107154.
[58] S.J. Mackwell, Oxidation kinetics of fayalite (Fe2SiO4), Phys. Chem. Miner. 19 (4) (1992) 220–228, https://doi.org/10.1007/BF00202311.
[59] A. Corcoran, P. Knutsson, F. Lind, H. Thunman, Mechanism for Migration and Layer growth of Biomass Ash on Ilmenite used for Oxygen carrier aided Combustion, Energy Fuel 32 (8) (2018) 8845–8856, https://doi.org/10.1021/acs.energyfuels.8b01888.
[60] H. He, X. Ji, D. Boström, R. Backman, M. Öhman, Mechanism of Quartz Bed Particle Layer Formation in Fluidized Bed Combustion of Wood-Derived Fuels, Energy Fuel 30 (3) (2016) 2227–2232, https://doi.org/10.1021/acs.energyfuels.5b02891.
[61] J. Bao, Z. Li, N. Cai, Promoting the reduction reactivity of ilmenite by introducing foreign ions in chemical looping combustion, Ind. Eng. Chem. Res. 52 (18) (2013) 6119–6128, https://doi.org/10.1021/ie400237p.
[62] X. Yang, et al., Interaction of ilmenite oxygen carrier with wheat straw ash during chemical looping combustion: Mechanisms and performance variation, Fuel 374, no. February (2024) 132434, https://doi.org/10.1016/j.fuel.2024.132434.
[63] P. Moldenhauer, M. Rydén, A. Lyngfelt, Testing of minerals and industrial by-products as oxygen carriers for chemical-looping combustion in a circulating fluidized-bed 300 W laboratory reactor, Fuel 93 (2012) 351–363, https://doi.org/10.1016/j.fuel.2011.11.009.
[64] L.H. Nuutinen, M.S. Tiainen, M.E. Virtanen, S.H. Enestam, R.S. Laitinen, Coating layers on bed particles during biomass fuel combustion in fluidized-bed boilers, Energy Fuel 18 (1) (2004) 127–139, https://doi.org/10.1021/ef0300850.
[65] V. Andersson, I. Staničić, X. Kong, H. Leion, T. Mattisson, J.B.C. Pettersson, Alkali desorption from ilmenite oxygen carrier particles used in biomass combustion, Fuel 359 (March) (2024), https://doi.org/10.1016/j.fuel.2023.130400.